On the origins of Earth rotation anomalies: New insights on the basis of both "paleogeodetic" data and Gravity Recovery and Climate Experiment (GRACE) data

W. R. Peltier[1] and Scott B. Luthcke[2]

Received 3 February 2009; revised 3 June 2009; accepted 5 August 2009; published 18 November 2009.

[1] The theory previously developed to predict the impact on Earth's rotational state of the late Pleistocene glaciation cycle is extended. In particular, we examine the extent to which a departure of the infinite time asymptote of the viscoelastic tidal Love number of degree 2, "k_2^T," from the observed "fluid" Love number, "k_f," impacts the theory. A number of tests of the influence of the difference in these Love numbers on theoretical predictions of the model of the glacial isostatic adjustment (GIA) process are explored. Relative sea level history predictions are shown not to be sensitive to the difference even though they are highly sensitive to the influence of the changing rotational state itself. We also explore in detail the accuracy with which the Gravity Recovery and Climate Experiment (GRACE) satellite system is able to observe the global GIA process including the time-dependent amplitude of the degree 2 and order 1 spherical harmonic components of the gravitational field, the only components that are significantly influenced by rotational effects. It is explicitly shown that the GRACE observation of these properties of the time-varying gravitational field is sufficiently accurate to rule out the values predicted by the ICE-5G (VM2) model of Peltier (2004). However, we also note that this model is constrained only by data from an epoch during which modern greenhouse gas induced melting of both the great polar ice-sheets and small ice sheets and glaciers was not occurring. Such modern loss of grounded continental ice strongly influences the evolving rotational state of the planet and thus the values of the degree 2 and order 1 Stokes coefficients as they are currently being measured by the GRACE satellite system. A series of sensitivity tests are employed to demonstrate this fact. We suggest that the accuracy of scenarios for modern land ice melting may be tested by ensuring that such scenarios conform to the GRACE observations of these crucial time-dependent Stokes coefficients.

Citation: Peltier, W. R., and S. B. Luthcke (2009), On the origins of Earth rotation anomalies: New insights on the basis of both ''paleogeodetic'' data and Gravity Recovery and Climate Experiment (GRACE) data, *J. Geophys. Res.*, *114*, B11405, doi:10.1029/2009JB006352.

1. Introduction

[2] The origins of highly significant anomalies in the Earth's rotational state, the so-called nontidal acceleration of the rate of planetary rotation and the secular drift (true polar wander) of the pole of rotation relative to the surface geography, respectively, have been associated for some time with the influence of the glacial isostatic adjustment (GIA) process [e.g., *Peltier*, 1982; *Sabadini and Peltier*, 1981; *Wu and Peltier*, 1984]. The former of these anomalies consists of a departure of the observed rate of change of the length of day from the rate of increase that would be caused solely by the action of tidal friction. Since the rate of change due to the action of tidal friction alone may be accurately estimated on the basis of the observed rate of recession of the Moon, using lunar laser ranging, and since the net increase in the length of day as a function of time may be inferred on the basis of the analysis of ancient eclipse observations [e.g., *Stephenson and Morrison*, 1995], one may infer the action of a nontidal component of the acceleration of rotation, which acts so as to slightly reduce the rate of increase of the length of day due to tidal friction, in the amount $(1.6 \pm 0.4) \times 10^{-22}$ rad s^{-1} over the past ~2500 years. This nontidal acceleration is equivalent to a value for the time dependence of the degree 2 zonal coefficient in the spherical harmonic expansion of Earth's gravitational field, commonly represented in terms of a parameter denoted $\dot{J}_2$, of approximately $(-2.67 \pm 0.15) \times 10^{-11}$ yr^{-1} [e.g., *Yoder et al.*, 1983; *Cheng et al.*, 1989; *Cheng and Tapley*, 2004]. Although a transient departure from this long timescale trend has been noted in apparent association with an especially strong

[1]Department of Physics, University of Toronto, Toronto, Ontario, Canada.
[2]NASA Goddard Space Flight Center, Planetary Geophysics Laboratory, Greenbelt, Maryland, USA.

Copyright 2009 by the American Geophysical Union.
0148-0227/09/2009JB006352$09.00

El Niño–Southern Oscillation event [*Cox and Chao*, 2002], following this event, the system recovered in such a way that the initial trend was reestablished.

[3] The second of the Earth rotation anomalies that has been connected to the ongoing action of the GIA process, namely, that associated with true polar wander, was initially measured by the International Latitude Service (ILS) using photo zenith tube observations of star transits. The value for the rate of polar wander reported by *Vincente and Yumi* [1969, 1970] using these data was $(0.95° \pm 0.15°)$ Myr^{-1}, a value that is close to the most recent estimation by *Argus and Gross* [2004] of 1.06° Myr^{-1}. Argus and Gross have suggested that the observed direction and speed of polar wander should be corrected for the influence of plate tectonic motions and that this could be a significant effect, depending on the assumptions on the basis of which the correction is made [see *Argus and Gross*, 2004, Table 1]. Whereas the ILS inference uncorrected for plate motion was that the ongoing polar wander was southward along the 75.5° west meridian, if the same data set is corrected by making the inference in the frame of reference in which the lithosphere exhibits no net rotation, then the corresponding speed and direction change slightly to 0.98° Myr^{-1} southward along the 79.9° west meridian. However, if the correction to these data is based on the "hot spot frame," then one obtains, from the ILS data, according to *Argus and Gross* [2004], the values 1.12° Myr^{-1} for the speed and southward along the 69° west meridian for the direction, a significant difference. The question as to the direction of true polar wander that has been characteristic of Earth's rotational state over the past century, based on the ILS and more recent data, may be just as important as the speed. The reason for this has to do with the use of the rotational anomalies to constrain the rate of melting of land ice near the poles that is occurring at present due to the action of greenhouse gas induced global warming. Depending on the polar wander prediction due to the continuing action of the GIA effect, there will exist a residual between this prediction and the modern observations that may be employed to constrain the rate and geographical locations of modern sources of land ice melting (Greenland, Alaska, Antarctica, small ice sheets and glaciers) as previously discussed by, e.g., *Peltier* [1998, Figure 46]. This issue has been further addressed by *Peltier* [2009] and will receive additional comment in the discussion to follow.

[4] The development of theoretical explanations for the above discussed anomalies in Earth rotation has been dominated by work over the past 2 decades that has suggested a close connection of them both to the GIA process. The earliest discussion of the impact on polar wander that should be expected due to time-dependent surface loading of a viscoelastic model of the Earth was that of *Munk and MacDonald* [1960], who employed a simple homogeneous model to suggest that wander of the pole could only occur in response to simultaneous variability in the surface mass load. This point was obscured in the later papers by *Nakiboglu and Lambeck* [1980, 1981] and *Sabadini and Peltier* [1981], whose analyses were based on the application of a homogeneous viscoelastic model similar to that employed by *Munk and MacDonald* [1960]. *Nakiboglu and Lambeck* [1980, 1981] and *Sabadini and Peltier* [1981], however, suggested that polar wander would continue on a homogeneous viscoelastic model of the Earth even after all temporal variations of the surface mass load had ceased. This significant error of interpretation was corrected by *Peltier* [1982] and *Wu and Peltier* [1984], who showed that, in the case of cyclic loading and unloading, as is appropriate for the computation of the GIA effect following the series of glacial loading and unloading events that have characterized the Late Quaternary period of Earth history [e.g., *Broecker and van Donk*, 1970], a homogeneous viscoelastic model would exhibit no polar wander once the surface mass load ceased to vary. The rotational response of a homogeneous viscoelastic model would therefore exhibit no memory of the past history of loading and unloading. This was traced to the fact that, in the special case of a homogeneous viscoelastic model, there exists an exact annihilation of the polar wander forced by the internal redistribution of mass due to the free relaxation Earth's shape and that forced by the deformation due to the changing rotation itself [see, e.g., *Wu and Peltier*, 1984, Figure 2].

[5] On the basis of the prior analysis of *Peltier* [1974, 1976], however, it was known that realistic viscoelastic models of the planetary interior were significantly more complex than could be accommodated by the homogeneous viscoelastic model of *Munk and MacDonald* [1960]. Whereas the relaxation under surface forcing of a homogeneous viscoelastic model of the Earth is described by a single relaxation time that is unique for each spherical harmonic degree in the deformation spectrum, realistically layered spherical viscoelastic models have a much more complex relaxation spectrum, a unique spectrum consisting of an (often essentially) finite number of modes for each spherical harmonic degree. *Peltier* [1982] and *Wu and Peltier* [1984] demonstrated that this realistic level of complexity endowed the Earth model with a memory of its history of surface loading and unloading such that the pole of rotation would continue to wander even after the surface load had ceased to vary. Deep-sea core oxygen isotopic data based on $\delta^{18}0$ measurements on benthic foraminifera were employed as the basis for the construction of a model of cyclic ice sheet loading and unloading of the continents, following the interpretation of such data as proxy for the variation of continental ice volume through time [*Shackleton*, 1967; *Shackleton and Opdyke*, 1973]. Analysis based on the application of rather crude models of the growth and decay of the Laurentian, Fennoscandian, and Antarctic ice sheets then demonstrated that both the speed and direction of true polar wander as well as the nontidal acceleration of rotation could be fit by the model and that the radial viscoelastic structure required to simultaneously fit both observations was essentially the same. This was construed to strongly suggest that both rotational anomalies might to be entirely explained as a consequence of the ongoing global GIA process.

[6] Since publication of the earliest results supporting this interpretation, considerably more refined analyses have been performed using models in which both the space-time dependence of the surface mass load and the radial viscoelastic structure of the Earth's interior have been modified so as to better fit the observational constraints. In a series of papers published in the early 1990s in particular, the ICE-4G (VM2) model of the GIA process was derived [*Peltier*,

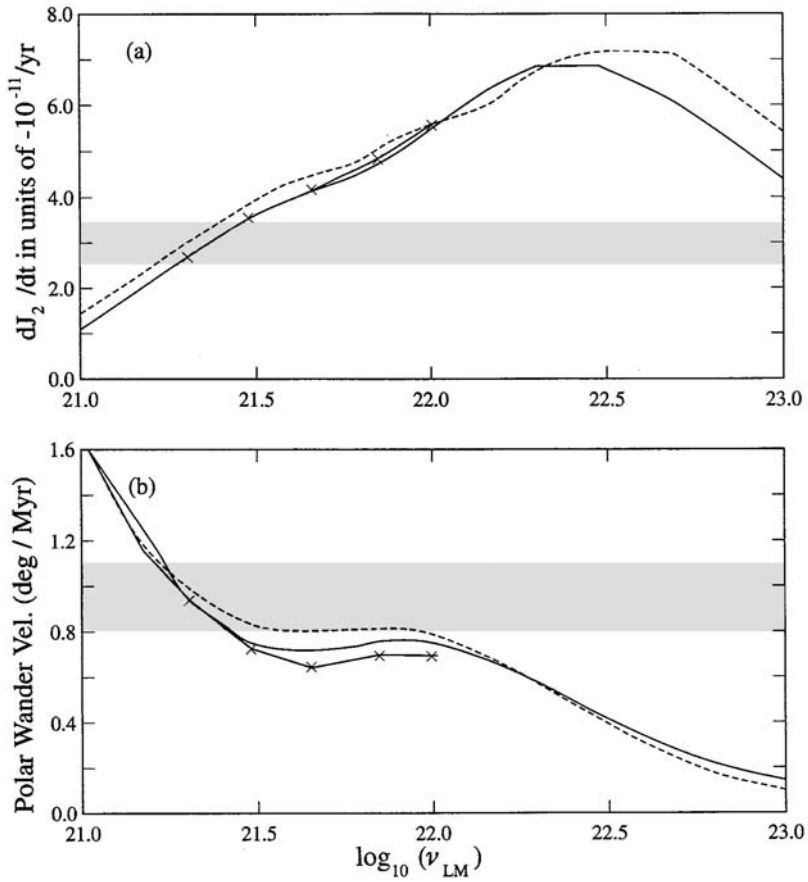

Figure 1. (a) $\dot{J}_2$ as a function of lower mantle viscosity with the upper mantle viscosity held fixed to the value of 10^{21} Pa s. (b) Same as Figure 1a but for polar wander speed. The shaded region represents the observationally constrained range. From *Peltier and Jiang* [1996]. Note that both Earth rotation anomalies are "explained" as a consequence of the glacial isostatic adjustment process by the same model of the radial variation of mantle viscoelasticity.

1994, 1996], a model that has been employed very widely as the basis for fixing the surface boundary conditions required for the reconstruction of ice age climates using modern general circulation models of the coupled atmosphere-ocean system [e.g., see *Pinot et al.*, 1999]. The application of the ICE-4G loading component of this model was further employed by *Peltier and Jiang* [1996] to investigate its ability to simultaneously explain both Earth rotation anomalies. The results in their paper, reproduced here as Figure 1, were based on a series of simplified radial viscoelastic structures that were employed to perform the calculations. In particular, the elastic structure of the Earth model was fixed to that of the preliminary reference Earth model (PREM) of *Dziewonski and Anderson* [1981], the upper mantle viscosity, υ_{UM}, was fixed to a value of 10^{21} Pa s, the lithospheric thickness was fixed to a value of 120 km, and the viscosity of the entire lower mantle υ_{LM} was varied through the range $\upsilon_{LM} = 10^{21}$ Pa s to $\upsilon_{LM} = 10^{23}$ Pa s. Inspection of Figure 1 will show that the radial variation of viscosity in this simple two-layer model that was required to fit both polar wander speed and $\dot{J}_2$ was essentially the same, confirming the previous results obtained with considerably simpler loading models. The ability of the GIA-based theory to simultaneously fit both rotational observables is extremely important. Because the $\dot{J}_2$ and polar wander data are dependent on entirely distinct elements of the moment of inertia tensor of the planet (see the analysis to follow), all of which are determined by the specific space-time history of continental ice sheet loading and unloading that is assumed as basis for the calculation, it would then be an extraordinary coincidence indeed if the GIA effect were not the correct primary explanation for both observables. There nevertheless persists in the literature [see, e.g., *Paulson et al.*, 2007, and references therein] the opinion to the effect that other influences may be important. The perspective adopted herein is that, unless it can be shown that the GIA process cannot simultaneously explain both observables, other influences are unlikely to be significant.

[7] Since the publication of these results, however, further improvements of the model have been achieved. By far the most important of these is the refinement of the history of surface mass loading denoted ICE-5G presented by *Peltier* [2004]. This paper will primarily focus on the implications of the latter refinement to the understanding of the implications of the Earth rotation observations. A sharp focus on the predictions of this model would appear to be warranted by virtue of the fact that its validity has been independently verified by *Paulson et al.* [2007], who, by

assuming the validity of loading history ICE-5G, infer a radial viscosity profile that is fully compatible with VM2 when a two-layer parameterization of the viscosity structure is assumed in which the interface is placed at the depth of the 660 km phase transformation.

[8] In section 2, we extend the theory previously developed as the basis on which predictions are made of the GIA-induced changes in Earth rotation. The focus will be on an issue recently raised by *Mitrovica et al.* [2005, hereafter MW], who have suggested that this theory is flawed as it was based on an inherently unstable mathematical formulation. This suggestion is herein shown to be incorrect. Their further contention appears to be that processes other than glacial isostatic adjustment are necessarily contributing in an important way to the determination of Earth's rotational response to the late Quaternary ice age cycle. It will also be argued herein that this suggestion is unfounded. In section 3, a detailed model of the time variations of the elements of the moment of inertia tensor of the planet is presented that is employed for the subsequently described analyses of the rotational response to the GIA process. Section 4 describes the results obtained for the prediction of the fundamental rotational observables for both simple layered viscosity models (section 4.1) and for the more realistic VM2 representation of this structure (section 4.2). In section 5 an investigation is presented of the extent to which Holocene observations of relative sea level (RSL) history may be employed to demonstrate the importance of the influence of rotational feedback, properly computed, to the accurate prediction of RSL history. Section 6 discusses the extent to which the time-dependent gravity field observations being delivered by the Gravity Recovery and Climate Experiment (GRACE) satellite system may be employed to further constrain the assumptions on which computations of the rotational response of the planet to the GIA process are performed. Conclusions that follow from the results of all these analyses are offered in section 7.

2. Theoretical Preliminaries

[9] Following a very brief review of established theory in sections 2.1 and 2.2, section 2.3 presents the mathematical basis of the considerable extension of this theory that will be employed in sections 2.2–6 (it is worth noting that a "grey literature proceedings volume" discussion of the results in section 2.3 is also available from *Peltier* [2008]).

2.1. Sea Level Histories on a Viscoelastic Planet Subject to Surface Mass Loading

[10] Because the Earth's shape is significantly deformed by the exchange of mass between the oceans and continents as continental ice sheets grow and decay, the space- and time-dependent variations of sea level that accompany this interaction are extremely complex. However, it is possible to exploit the fact that the ratio of the changes in local radius of the Earth to its mean radius are small to accurately predict the variations of sea level caused by an assumed known history of the evolution of land ice thickness. Such predictions are made by solving an integral equation that I have come to refer to as the sea level equation (SLE). A primitive version of the SLE was first solved by *Clark et al.* [1978] and *Peltier et al.* [1978], based on the work of *Peltier* [1974, 1976], *Peltier and Andrews* [1976], and *Farrell and Clark* [1976]. Given a history of continental ice sheet thickness variations $I(\theta, \lambda, t)$, solution of the SLE delivers the space- and time-dependent field $S(\theta, \lambda, t)$ which represents the variation of the level of the sea relative to the continuously deforming surface of the solid Earth. In these expressions, θ is latitude, λ is longitude, and t is time. The sea level equation that relates these quantities is

$$S(\theta,\lambda,t) = C(\theta,\lambda,t)\left[\int_{-\infty}^{t} dt' \iint_{\Omega} d\Omega' \left\{L(\theta',\lambda',t')\, G_{\varphi}^{L}(\varphi, t-t') + \Psi^{R}(\theta',\lambda',t')\, G_{\varphi}^{T}(\varphi, t-t')\right\} + \frac{\Delta\Phi(t)}{g}\right]. \tag{1}$$

In (1), $C(\theta, \lambda, t)$ is the "ocean function" as defined originally by *Munk and MacDonald* [1960], which is unity over the oceans and zero over the land. This is time-dependent because of the migration of the coastlines that occurs as water is added to (or removed from) the ocean basins. A highly accurate iterative method for the computation of the time dependence of C was presented by *Peltier* [1994]. Also in (1), the space- and time-dependent function L is the surface mass load per unit area which may be decomposed to write

$$L(\theta, \lambda, t) = \rho_I\, I(\theta, \lambda, t) + \rho_w\, S(\theta, \lambda, t), \tag{2}$$

in which ρ_I and ρ_w are the densities of ice and water, respectively. In the Green functions G_{φ}^{L} and G_{φ}^{T}, the angle ϕ is the angular separation between the source point with coordinates (θ', λ') and field point with coordinates (θ, λ). The $\psi^{R}(\theta, \lambda, t)$ is the variation of the centrifugal potential due to the changing rotational state of the planet which may be written, to first order in perturbation theory, following *Dahlen* [1976], as

$$\Psi^{R}(\theta, \lambda, t) = \Psi_{00}\, Y_{00}(\theta, \lambda, t) + \sum_{m=-1}^{+1} \Psi_{2m}\, Y_{2m}(\theta, \lambda, t) \tag{3}$$

with

$$\Psi_{00} = \frac{2}{3}\omega_3(t)\,\Omega_0 a^2, \tag{4a}$$

$$\Psi_{20} = -\frac{1}{3}\omega_3(t)\,\Omega_0\, a^2\sqrt{4/5}, \tag{4b}$$

$$\Psi_{2,-1} = (\omega_1 - i\omega_2)\left(\Omega_0\, a^2/2\right)\sqrt{2/15}, \tag{4c}$$

$$\Psi_{2,+1} = -(\omega_1 + i\omega_2)\left(\Omega_0 a^2/2\right)\sqrt{2/15}. \tag{4d}$$

The $\omega_i(t)$ in equations (4) represent the time-dependent variations in the three Cartesian components of the angular

velocity vector of the planet, whereas Ω_0 is the unperturbed angular velocity of the Earth and a is the mean radius. The remaining terms in (1) consist of the surface mass loading and tidal potential loading Green functions for the perturbations of the gravitational potential which have the mathematical representations (see *Farrell* [1972] for the equivalent elastic, and therefore time-independent, forms):

$$G_\varphi^L(\varphi, t) = \frac{a}{m_e} \sum_{\ell=o}^{\infty} \left[1 + k_\ell^L(t) - h_\ell^L(t)\right] P_\ell(\cos\varphi) \quad (5a)$$

$$G_\varphi^T(\varphi, t) = \frac{a}{g} \sum_{l=0}^{¥} \left[1 + k_l^T(t) - h_l^T(t)\right] P_l(\cos\varphi), \quad (5b)$$

in which the k_ℓ^L (t) and h_ℓ^L (t) are viscoelastic surface mass load Love numbers and the k_ℓ^T (t) and h_ℓ^T (t) are corresponding tidal potential loading Love numbers. For impulsive point mass loading, *Peltier* [1976, 1985] has shown that these time domain Love numbers may be expressed as normal mode expansions of the form (for two examples only)

$$k_\ell^L(t) = k_\ell^{L,E}\,\delta(t) + \sum_{j=1}^{M} q_j^\ell\, e^{-s_j^\ell t} \quad (6a)$$

$$k_\ell^T(t) = k_\ell^{T,E}\,\delta(t) + \sum_{j=1}^{M} q_j'^\ell\, e^{-s_j^\ell t}, \quad (6b)$$

in which the s_j^ℓ are inverse relaxation times determined by the position of "poles" in the complex plane of the Laplace transform variable s as the zeros of an appropriate secular function [*Peltier*, 1985], and the amplitudes of the individual modes of exponential relaxation are determined by the residues at these poles. In this paper special attention will be focused on the Love number k_2^T. The reason for this will become clear in what follows. In the domain of the Laplace transform variable s this Love number has the form

$$k_2^T(s) = k_2^{T,E} + \sum_{j=1}^{M} \frac{q_j'^2}{s + s_j^2}. \quad (6c)$$

Especially critical is the comparison of this Laplace transform domain form of the impulse response Love number and the time-dependent form of the Heaviside response Love number which is obtained by convolution of equation (6b) with a unit Heaviside step function, namely,

$$k_2^{T,H}(t) = k_2^{T,E} + \sum_{j=1}^{M} \frac{q_j'^2}{s_j^2}\left(1 - e^{-s_j^2 t}\right). \quad (6d)$$

Comparison of (6c) and (6d) will show that the infinite time limit of the Heavside response (6d) is identical to the value of the Laplace transform of the impulse response evaluated at s = 0. This is critical to the understanding of what is to follow as it means that in the limit of infinite time after the application of a constant tidal forcing associated with a fixed rate of Earth rotation, the Love number that describes the flattening of planetary shape may be evaluated as the Laplace transform of the impulse response at $s = 0$.

2.2. Computation of the Rotational Response of the Earth to the GIA Process

[11] Determination of the ω_i in equations (4) requires solution of the classical Euler equation describing the conservation of angular momentum of a system subjected to no external torques as

$$\frac{d}{dt}\left(J_{ij}\,\omega_i\right) + \in_{ijk}\ \omega_j\, J_{k\ell}\,\omega_\ell = 0. \quad (7)$$

The J_{ij} in (7) are the elements of the moment of inertia tensor whereas $\in_{ijk}$ is the Levi-Civita (alternating) tensor. Solutions to (7) accurate to first order in perturbation theory may be constructed by expanding

$$\omega_i = \Omega_0\,(\delta_{i3} + m_i);\ m_i = \omega_i / \Omega_0, \quad (8a)$$

$$J_{11} = A + I_{11}, \quad (8b)$$

$$J_{22} = B + I_{22}, \quad (8c)$$

$$J_{33} = C + I_{33}, \quad (8d)$$

$$J_{ij} = I_{ij},\ i \neq j. \quad (8e)$$

Substitution of these expansions into equation (7), keeping only first-order terms, delivers the linear decoupled system for polar wander and the length of day, respectively [see *Munk and McDonald*, 1960], as

Polar wander

$$\frac{\mathrm{d}m_1}{\mathrm{d}t} + \frac{(C - B)}{A}\,\Omega_o\, m_2 = \Psi_1 \quad (9a)$$

$$\frac{\mathrm{d}m_2}{\mathrm{d}t} + \frac{(C - A)}{B}\,\Omega_o\, m_1 = \Psi_2 \quad (9b)$$

Length of day

$$\frac{\mathrm{d}m_3}{\mathrm{d}t} = \Psi_3, \quad (9c)$$

in which the so-called "excitation functions" are

$$\Psi_1 = \left(\frac{\Omega_o}{A}\right) I_{23} - \frac{(\mathrm{d}I_{13}/\mathrm{d}t)}{A}, \quad (10a)$$

$$\Psi_2 = -\left(\frac{\Omega_o}{B}\right) I_{13} - \frac{(\mathrm{d}I_{23}/\mathrm{d}t)}{B}, \quad (10b)$$

$$\Psi_3 = -\left(\frac{I_{33}}{C}\right). \quad (10c)$$

The methodology best suited to the solution of these time domain equations is that based on the Laplace transform. This has most recently been reviewed by *Peltier* [2007b] and no useful purpose will be served by reproducing the analysis here. The final result, in terms of the Laplace transform variable s is simply, in terms of the vector $\mathbf{m}$ (s) = ($m_1(s)$,$m_2(s)$) for polar wander:

$$\mathbf{m}(s) = \frac{\mathbf{\Psi}^L(s)}{\left[1 - \left(k_2^T(s)/k_f\right)\right]} = H(s)\left(I_{13}^{\text{Rigid}}(s),\ I_{23}^{\text{Rigid}}(s)\right), \tag{11a}$$

where

$$\mathbf{\Psi}^L(s) = \left[\left(\frac{\Omega_o}{A\,\sigma}\right)\left(1 + k_2^L(s)\right)\left(I_{13}^{\text{Rigid}}(s),\ I_{23}^{\text{Rigid}}(s)\right)\right] \tag{11b}$$

and in which the fluid Love number k_f is defined as

$$k_f = \left(\frac{3G}{a^5\,\Omega_o^2}\right)(C - A), \tag{11c}$$

in which $A = B$ has been assumed and $k_2^T(s)$ is the tidal potential loading Love number of degree 2, the parameter that will be seen to play a crucial role in what follows and whose form has been written explicitly in equation (6c). The parameter σ in equations (11a)–(11c) is the frequency of the Chandler wobble of a rigid model of the Earth which is given by $[(C - A)/C]\Omega_0$. Especially crucial for the arguments to be presented is the so-called "fluid Love number" k_f, the value of which is determined entirely on the basis of the well known equatorial flattening of the planet that is represented by the difference between the polar and equatorial moments of inertia (C-A) in equation (11c). Substituting in (11c) for Newton's gravitational constant G, the Earth's radius a (for which we will take the equatorial value), the present-day rate of angular rotation Ω_o and the polar and equatorial moments of inertia C and A, respectively, taking all data from the tabulation of *Yoder* [1995], one obtains for the value of k_f that

$$k_f \cong 0.9414, \tag{12}$$

a value that deviates marginally from the value $k_f = 0.9382$ employed in MW. An important part of the discussion to follow will involve understanding of the connection between k_f and $k_2^T(s = 0)$ the asymptotic value of the viscoelastic tidal loading Love number of degree 2 for $s = 0$. Since the solution for the length of day variations is relatively simple it will not be repeated here. The Laplace transform variable dependent moment of inertia tensor perturbations in equations (11), which are superscripted "rigid" are those that would be caused by the variations in surface mass load if the planet were a rigid body undeformable by either GIA or the changing rotational state.

2.3. Alternative Theoretical Formulations for Determining Earth's Rotational Response to the GIA Process

[12] From equations (11a)–(11c) it will be clear that the solution for the polar wander vector $\mathbf{m}$(s) will depend critically on the ratio $k_2^T(s)/k_f$. This fact was more fully exposed in the analysis of *Peltier* [1982] and *Wu and Peltier* [1984], who rewrote the Laplace transform domain forms of $k_2^T(s)$ and $k_2^L(s)$ as [e.g., see *Wu and Peltier*, 1984, equation 61]

$$k_2^T(s) = k_2^T(s = 0) - s\sum_{j=1}^{N}\frac{\left(q_j'/s_j\right)}{(s + s_j)} \tag{13a}$$

$$k_2^L(s) = (-1 + \ell_s) - s\sum_{j=1}^{N}\frac{(q_j/s_j)}{(s + s_j)}, \tag{13b}$$

in which the superscript $\ell = 2$ on q_j^2, r_j^2, s_j^2 has been suppressed for convenience. Substituting (13a) into (11), this may be rewritten as

$$\mathbf{m}(s) = \frac{\mathbf{\Psi}^L(s)}{\left[1 - \dfrac{k_2^T(s = 0)}{k_f}\right] + \dfrac{s}{k_f}\displaystyle\sum_{j=1}^{N}\frac{\left(q_j'/s_j\right)}{(s + s_j)}}. \tag{14}$$

In discussing the formal inversion of (14) into the time domain, it will prove important to distinguish the results of an approximate solution from those for the full solution.

2.3.1. "Equivalent Earth Model" Approximation of *Munk and McDonald* [1960]

[13] Since the surface of the Earth is broken into a large number of individually rigid lithospheric "plates" whose boundaries are in general weak, it should be the case on physical grounds that, at spherical harmonic degree 2, the effective $k_2^T(s = 0)$ will be close to k_f since in this infinite time limit the absence of strength at plate boundaries will enable the planet as a whole to adjust to the tidal (rotational) forcing as if the planet had no surface lithosphere at all. From a mathematical perspective it is important to note the following Tauberian theorem [see, e.g., *Widder*, 1946] that relates the infinite time limit of a function $f(t)$, say, to its Laplace transform $F(s)$, say, as

$$\lim_{t\to\infty} f(t) = \lim_{s\to 0} sF(s). \tag{15}$$

The suggestion by MW that the solution (14) subject to the assumption $k_f = k_2^T(s = 0)$ represents in some sense an "unstable formulation" of the theory for the rotatonal response seems to imply that they believe that this solution will diverge to infinity in the limit of long time as a consequence of linear instability. That this is incorrect follows from the above Tauberian theorem. Since we must multiply the right hand side of (14) by s and take the limit $s \to 0$ in order to determine the infinite time limit of the solution for $m(t)$, it will be clear that this multiplication cancels the factor s in the denominator of (14) thus rendering the $t \to \infty$ limit finite. There is therefore no "instability" in this equivalent Earth Model formulation of the problem.

[14] Now the actual value of the parameter $k_2^T(s = 0)$ relative to k_f is therefore of considerable importance and this value is a function of the effective thickness of the litho-

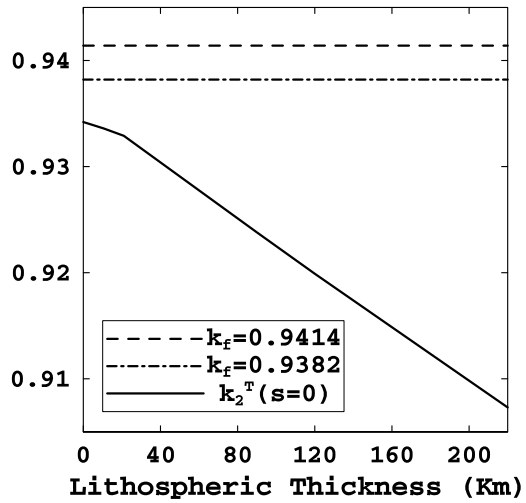

Figure 2. The infinite time asymptotic value of the tidal potential loading Love number of degree 2 is shown as a function of lithospheric thickness. This infinite time limit is identical to the limit in which the Laplace transform variable s equals zero. Also shown are two plausible values of the fluid Love number k_f which is a constant determined by the observed flattening of Earth's shape as measured by the difference between the polar and equatorial moments of inertia ($C - A$). Note that the difference between k_2^T (s = 0) and k_f in the limit of zero lithospheric thickness is <1% for either value of the fluid Love number. See text for further discussion.

sphere in the limit of long time (note that the infinite time response of a tidal Love number in the case of a constant tidal forcing applied instantaneously and maintained is identical to the Laplace transform of the same Love number evaluated at $s = 0$; see *Peltier* [1982, equation 3.32] and equations (6b) and (6d)). That the value of this parameter does tend toward k_f as the thickness of the lithosphere tends to zero in the spherically symmetric theory is clear on the basis of Figure 2 [see also *Wu and Peltier*, 1984, Table 5]. On the basis of Figure 2 it is notable that the deviation of k_2^T ($s = 0$) from k_f, at zero lithospheric thickness, irrespective of which of the two previously quoted values of k_f is more accurate, is by less that 1% (this slight deviation is most probably best understood to be a consequence of the fact that the density structure within the real Earth deviates somewhat from spherical symmetry as a consequence of the lateral heterogeneity associated with the convective mixing process). The mathematical methods required to invert equation (14) under the assumption

$$1 - \frac{k_2^T\ (s\ =\ 0)}{k_f} \equiv 0 \tag{16}$$

were presented by *Peltier* [1982] and *Wu and Peltier* [1984] and will not be repeated here.

2.3.2. A Formulation That Retains the Difference Between k_2^T (s = 0) and k_f

[15] In this case the assumption k_2^T ($s = 0$) = k_f that is at the heart of the "equivalent Earth model" approach is abandoned and the Laplace transform domain impulse response is then

$$H\,(s)\ =\ \left(\frac{\Omega_o}{A\,\sigma}\right)\ \frac{1\ +\ k_2^L\,(s)}{\dfrac{s}{k_f}\displaystyle\sum_{j=1}^{N}\frac{\left(q_j\,/\,s_j\right)}{\left(s\ +\ s_j\right)}\ +\ \varepsilon} \tag{17a}$$

where we have defined the parameter

$$\varepsilon\ =\ 1\ -\ \frac{k_2^T\ \ (s\ =0)}{k_f}\,. \tag{17b}$$

As will become clear, even though ε is a small quantity (especially in the case that the finite thickness of the lithosphere may be neglected in the limit $t \to \infty$), retaining it in expression (17a) for the impulse response could have a significant impact on the solution as the rotational response of the system is modified. The construction of the solution for the time domain form of the impulse response $H(t)$ proceeds in this case as in that based on the equivalent Earth model assumption, although the result differs significantly from a mathematical perspective. The derivation of the exact solution for the impulse response in this case is original to this paper and is much more than a minor variation on previous attempts to discuss this issue such as that contained in MW where no detailed analysis was presented. In the construction of this more general solution it is useful to make the distinction between the Chandler wobble frequency of a rigid model of the Earth, σ, and the Chandler wobble frequency of a viscoelastic model σ_o, by employing the definition

$$\sigma_0 = \frac{\left(k_2^T(s=0) - k_2^{TE}\right)}{k_2^T(s=0)}\sigma. \tag{18}$$

We may then rewrite the expression for $H(s)$ as

$$H\,(s)\ =\ \left(\frac{\Omega}{A\ \sigma_o}\right)\ \frac{\left(1\ +\ k_2^L\ (s)\right)}{\left(\left(1\ -\ \varepsilon\right)s\displaystyle\sum_{i=1}^{N}\frac{g_j}{s\ +\ s_j}\right)\ +\ \varepsilon'} \tag{19a}$$

with

$$\varepsilon'\ =\ \varepsilon\ \frac{\sigma}{\sigma_0} \tag{19b}$$

and

$$g_j\ =\ \frac{q_j'\,/\,s_j}{\displaystyle\sum_j\left(q_j'\,/\,s_j\right)}\,. \tag{19c}$$

The inversion of H(s) into the time domain now proceeds by expanding the sum in the denominator of (19a) in the form

$$\sum_{j=}^{N}\frac{g_j}{\left(s\ +\ s_j\right)}\ =\ \frac{Q_{N\,-\,1}\,(s)}{\displaystyle\prod_{j=1}^{N}\left(s\ +\ s_j\right)}\ =\ \frac{\displaystyle\prod_{j=1}^{N-1}\left(s\ +\ \lambda_j\right)}{\displaystyle\prod_{j=}^{N}\left(s\ +\ s_j\right)}, \tag{20}$$

since $\sum_j g_j \equiv 1$ Then we have, suppressing for the moment the factor $(\Omega_0/A\sigma_0)$,

$$H(s) = \frac{\prod_{j=1}^{N}(s+s_j)\left[1+k_2^L(s)\right]}{(1-\varepsilon)s\prod_{i=1}^{N-1}(s+\lambda_i)+\varepsilon'\prod_{j=1}^{N}(s+s_j)}. \quad (21)$$

Now substituting for the function $1 + k_2^L(s)$ from (14b) we obtain

$$H(s) = \frac{\prod_{j=1}^{N}(s+s_j)\,\ell_s}{(1-\varepsilon)s\prod_{i=1}^{N-1}(s+\lambda_i)+\varepsilon'\prod_{i=1}^{N}(s+s_i)} + \sum_{j=1}^{N}\frac{(-q_j/s_j)\,s\prod_{i\neq j}^{N}(s+s_i)}{(1-\varepsilon)s\prod_{i=1}^{N-1}(s+\lambda_i)+\varepsilon'\prod_{i=1}^{N}(s+s_i)} \quad (22a)$$

or

$$H(s) = \frac{\prod_{j=1}^{N}(s+s_j)\,\ell_s}{(1-\varepsilon+\varepsilon')\prod_{i=1}^{N}(s+\kappa_i)} + \sum_{j=1}^{N}\frac{(-q_j/s_j)\,s\prod_{i\neq j}^{N}(s+s_j)}{(1-\varepsilon+\varepsilon')\prod_{i=1}^{N}(s+\kappa_i)}. \quad (22b)$$

Where now the κ_i are the N roots of the polynomial in the denominator of the two terms in (22a). This expression for the impulse response may be further reduced by rewriting the ratios of products as follows:

$$\frac{\prod_{j=1}^{N}(s+s_j)}{\prod_{j=1}^{N}(s+\kappa_i)} = 1 - \frac{q'(s)}{\prod_{i=1}^{N}(s+\kappa_i)}, \quad (23a)$$

where now

$$q'(s) = \prod_{j=1}^{N}(s+\kappa_i) - \prod_{j=1}^{N}(s+s_j) \quad (23b)$$

$$\frac{s\prod_{i\neq j}^{N}(s+s_i)}{\prod_{j=1}^{N}(s+\kappa_i)} = 1 - \frac{R_j'(s)}{\prod_{i=1}^{N}(s+\kappa_i)} \quad (24a)$$

with

$$R_j'(s) = \prod_{i=1}^{N}(s+\kappa_i) - s\prod_{i\neq j}^{N}(s+s_i). \quad (24b)$$

We then have, for the Laplace transform of the impulse response, the expression

$$H(s) = \frac{\ell_s}{(1-\varepsilon+\varepsilon')}\left\{1 - \frac{q'(s)}{\prod_{i=1}^{N}(s+\kappa_i)}\right\} + \frac{1}{(1-\varepsilon+\varepsilon')}\sum_{j=1}^{N}\left(-\frac{r_j}{s_j}\right)\left\{1 - \frac{R_j'(s)}{\prod_{i=1}^{N}(s+\kappa_i)}\right\} \quad (25a)$$

or

$$H(s) = \frac{\ell_s - \sum_{j=1}^{N} r_j/s_j}{(1-\varepsilon+\varepsilon')} - \frac{\ell_s\, q'(s)}{(1-\varepsilon+\varepsilon')\prod_{i=1}^{N}(s+\kappa_i)} + \frac{1}{(1-\varepsilon+\varepsilon')}\sum_{j=1}^{N}\frac{(q_j/s_j)\,R_j'(s)}{\prod_{i=1}^{N}(s+\kappa_i)}. \quad (25b)$$

Denoting

$$\ell_s - \sum_{j=1}^{N} r_j/s_j = 1 + k_2^{LE} = D_1,$$

say, we may then further reduce the expression for the impulse response to

$$H(s) = \frac{D_1}{(1-\varepsilon+\varepsilon')} - \frac{1}{(1-\varepsilon+\varepsilon')} \cdot \left\{\frac{\ell_s\, q'(s) - \sum_{j=1}^{N}(q_j/s_j)\,R_j'(s)}{\prod_{i=1}^{N}(s+\kappa_i)}\right\}. \quad (26)$$

The inverse Laplace transform of this expression is such that the solution in the present case, in which $k_2^T(s=0) \neq k_f$, is just:

$$m_1(t) = \frac{1}{(1-\varepsilon+\varepsilon')}\left(\frac{\Omega_o}{A\sigma_o}\right) \cdot \left\{\left[\ell_s - \sum_{j=1}^{N}\frac{r_j}{s_j}\right] I_{13}^{\text{Rigid}}(t) + \sum_{i=1}^{N} E_i'\, e^{-\kappa_i t} * I_{13}^{\text{Rigid}}(t)\right\} \quad (27a)$$

$$m_2(t) = \frac{1}{(1-\varepsilon+\varepsilon')}\left(\frac{\Omega_o}{A\sigma_o}\right) \cdot \left\{\left[\ell_s - \sum_{j=1}^{N}\frac{r_j}{s_j}\right] I_{23}^{\text{Rigid}}(t) + \sum_{i=1}^{N} E_i'\, e^{-\kappa_i t} * I_{23}^{\text{Rigid}}(t)\right\}, \quad (27b)$$

where

$$E'_i = \left\{ -\ell_s q'(-\kappa_i) + \sum_{j=1}^{N} \frac{r_j}{s_j} R'_j(-\kappa_i) \right\} / \prod_{i=j}^{N} (\kappa_j - \kappa_i). \tag{27c}$$

The components of the polar wander velocity vector are obtained simply by time differentiation of equations (27a) and (27b). It is useful to compare the result in (27) to the equivalent Earth model case. In the limit $\varepsilon \to 0$ we have $\kappa_N = 0$ and $\kappa_i = \lambda_i$ which are the $N-1$ relaxation times that govern the system in this limit [see, e.g., *Peltier*, 1982; *Wu and Peltier*, 1984]. In this case, the parameter E'_N in the above becomes

$$E'_N = -\frac{\ell_1 q(o)}{\prod_{j=1}^{N-1} (\kappa_j - \kappa_N)} = -\frac{\ell_s q(o)}{\prod_{j=1}^{N-1} \lambda_i}, \tag{28}$$

and the equivalent Earth model result is fully recovered. The mathematical analysis leading to the result for the polar wander speed prediction embodied in equations (27) is original to this paper.

[16] In order to compare the temporal histories of the rotational anomalies in the two cases, it will be important to proceed by keeping as many features of the Earth model fixed as possible. To this end and for the remainder of this paper, we will focus primarily on the VM2 viscosity model of *Peltier* [1996] that will be employed together with the PREM radial elastic structure of *Dziewonski and Anderson* [1981]. However, we will also discuss the results for simple two-layer viscosity models that may be directly compared to the earlier results shown on Figure 1. Equally important, of course, will be the model of glaciation and deglaciation that is employed to represent the surface mass load forcing. This model is briefly summarized in section 3.

3. ICE-5G-Based Model of the Late Pleistocene Glacial Cycle

[17] For the purpose of the analyses of the rotational response to the GIA process to be discussed in sections 4–6, we will employ a model of the late Pleistocene glaciation cycle based primarily on the ICE-5G (VM2) model of *Peltier* [2004]. Since a detailed discussion of the construction of this model is available from *Peltier* [2004], this will not be repeated here. However, it will be important to understand the basic characteristics of the geographical distribution of LGM land ice. These are described on Figure 3 where this distribution is described in terms of time series of the contributions to eustatic sea level rise from each of the main deglaciation centers. Results are shown not only for ICE-5G but also for the precursor model ICE-4G. Notable is the fact that the version of the ICE-4G model to be employed here has about 10% less mass than ICE-5G (the original version of the ICE-4G model was presented by *Peltier* [1994] and this had similar mass to that in ICE-5G. The modified form being employed herein was first adopted by *Peltier* [2002a] in order to correct for the excess mass that was assumed in the original model to have melted from Antarctica). More important, however, is the fact that a very significant shift of mass from the Eurasian sector to North America has been implemented in the ICE-5G reconstruction. The reasons for this were fully documented by *Peltier* [2004]. An interesting and important characteristic of the ICE-5G (VM2) model is that the deglaciation of Antarctica is such that the continent is assumed not to lose mass until the onset of meltwater pulse 1b, a pulse defined by a period of rapidly increasing sea level recorded in the Barbados data set that occurs at the end of the Younger Dryas period. This aspect of the ICE-5G reconstruction has recently been confirmed by *Domack et al.* [2005] and *Leventer et al.* [2006], who have carefully dated the timing of the recommencement of marine shelf sedimentation that occurred as the Antarctic ice sheet pulled back from the shelf break in response to the rise in sea level that was driven by the melting of northern hemisphere land ice. The spatial distribution of continental ice sheet thickness as a function of time for the ICE-5G (VM2) v1.2 model is currently available to interested users at http://www.atmosp.physics.utoronto.ca/~peltier/data.php

[18] The main constraint on the total mass of LGM ice is provided by the post glacial history of relative sea level change recorder in the coral sequences from the island of Barbados in the Caribbean Sea. This record, as recently extended by *Peltier and Fairbanks* [2006], is shown on Figure 4 where it is compared to the prediction for this site based on the solution to the SLE and to the "ice-equivalent" eustatic history based solely on the unloading of the continents caused by disappearing land ice across the glacial-interglacial transition and under the assumption that the area of the ocean basins remained unchanged in this process. Further discussion is provided in Figure 4 caption. Assuming that one may approximate the late Pleistocene ice age cycle by a perfectly periodic sequence of ICE-5G based pulses, one may construct time series for each of the elements of the moment of inertia tensor needed to compute the rotational response of the planet. The temporal form of a single pulse is presented in the inset to Figure 4 where the ICE-5G form is compared to an inference by *Waelbroeck et al.* [2002].

[19] Time series for the evolution of the elements of the moment of inertia tensor required to implement the theory for the rotational response described in section 4 are shown on Figure 5. These are based on the assumption that the complete history may be represented by a sequence of pulses of either ICE-4G or ICE-5G form. A detailed discussion of the construction of these time series is given by *Peltier* [2007b].

4. Assessing the Differences Between the Predictions of the Alternative Theories for GIA-Induced Rotational Anomalies

[20] The results to be presented in what follows will include not only analyses of the ICE-4G (VM2) and ICE-5G (VM2) models as a function of a crucial parameter Δ to be defined below, but also presentation of a sequence of results for the same two-layer parameterizations of the radial viscosity structure as were employed to produce the original results shown on Figure 1. The results for such two-layer models will be discussed first.

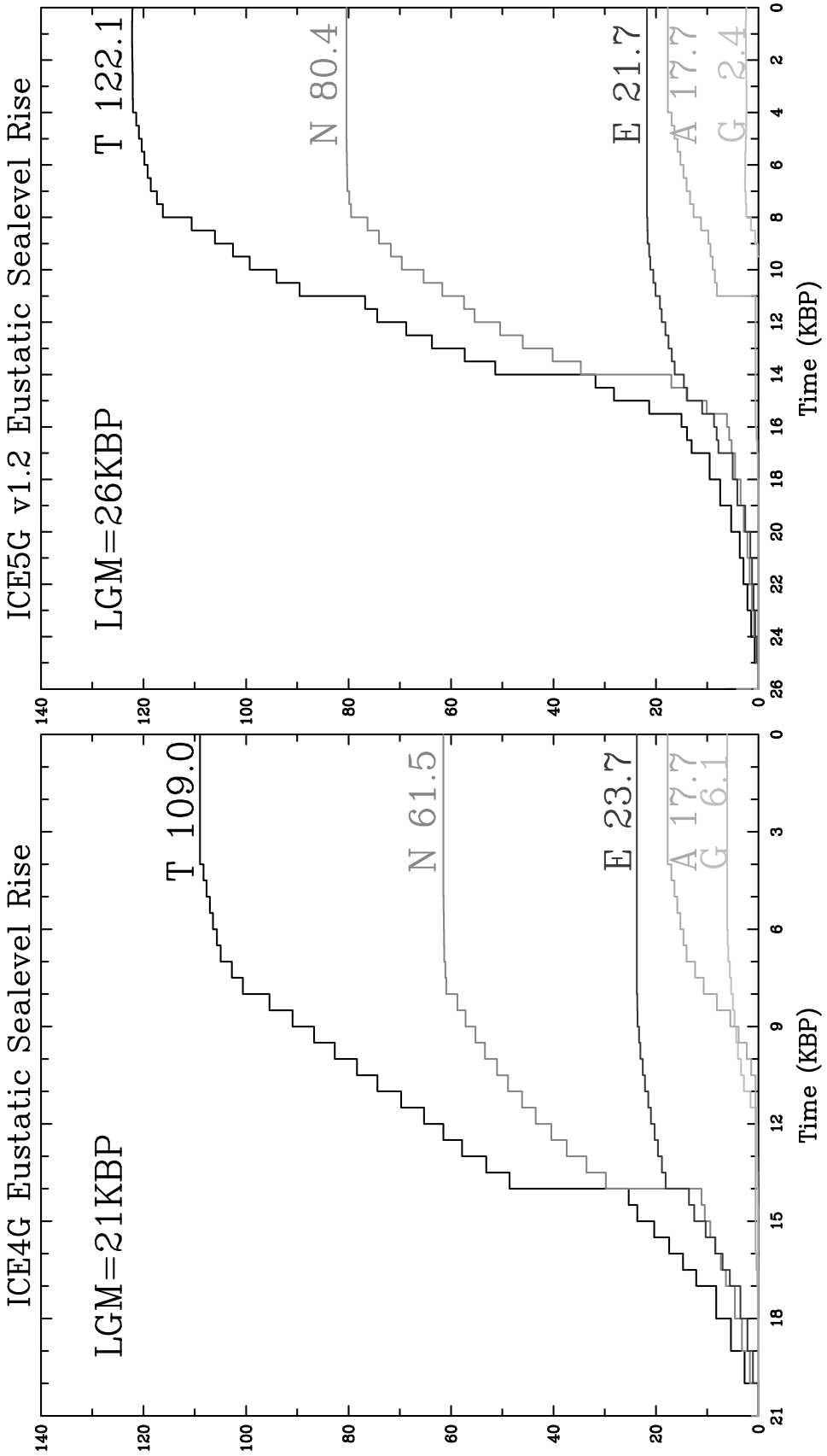

Figure 3. Eustatic sea level curves for the ICE-4G and ICE-5G V1.2 models of the last glacial-interglacial transition. Note that the most significant difference between these models concerns the net eustatic rise from LGM to present. For this version of the ICE-4G model, for which the reconstruction has been performed using the method described by *Peltier* [2005] in which the "implicit ice" methodology is not employed, the net eustatic rise (T) is 109.0 m. For the ICE-5G v1.2 model, on the other hand, the net eustatic rise is 122.1 m. Also evident is the very significant increase in ice mass located over the North American continent (the component denoted "N"; E denotes Eurasia, A denotes Antarctica and South America, and G denotes Greenland). The increase in North American ice mass is partly accounted for by decreases in both Greenland and Eurasia). Also notable is the fact that in the ICE-5G v1.2 model the deglaciation of Antarctica is assumed to begin very abruptly at the time of occurrence of meltwater pulse 1b in the Barbados sea level record. See the text for further discussion.

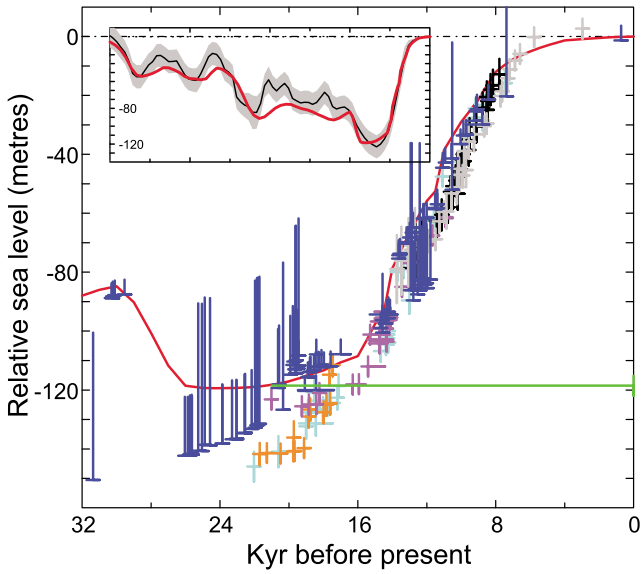

Figure 4. The fit of the predicted relative sea level history at the island of Barbados to the extended coral-based data set from this location tabulated by *Peltier and Fairbanks* [2006]. The blue symbols with error bars of various lengths represent these new Barbados data, the data represented by the shorter error bars of 5 m length are derived from the *Acropora palmate* species of coral that provide the best constraints on sea level. The data represented by the error bars on intermediate 20 m length derive from the *Montastraea annularis* species of coral. The data represented by the longest error bars derive either from *Porites asteroids* species or the *Diploria* species. The green horizontal line denotes the 118.7 m depth level which is the level corresponding to the samples of LGM age if LGM is assumed to have occurred at the conventionally assumed age of 21,000 years (ago). In order to fit this observational datum the eustatic depression of sea level at that age is almost precisely equal to the depth at which the sample of LGM age is found. This is a consequence of the fact that the Barbados record of relative sea level is an excellent approximation to eustatic sea level history itself. The inset shows the comparison between the eustatic history of the ICE-5G model and the complete 10^5 year glacial cycle with that inferred by *Waelbroeck et al.* [2002] based on benthic $\delta^{18}0$ records corrected for the influence of the change in abyssal ocean temperature. The colored crosses are the estimates of ice equivalent eustatic sea level proposed by *Lambeck and Chappell* [2001] which are in conflict with the Barbados constraints and thereby ruled out as plausible.

4.1. Differences in Model Predictions for Two-Layer Viscosity Parameterizations

[21] Figure 6 shows results for both the nontidal acceleration and polar wander speed for the ICE-5G loading history when the upper mantle viscosity is held fixed to the value of $\sim 0.4 \times 10^{21}$ Pa s that is characteristic of the VM2 model of *Peltier* [1994, 1996] and the lower mantle viscosity is varied through a wide range of values. The words "rotation included" on Figure 6 indicate that the full influence of the redistribution of water in the ocean basins due to the changing rotational state of the planet has been accounted for in the input time series for the elements of the moment of inertia tensor. Of particular importance for the purpose of this paper is the sensitivity of these predictions of polar wander speed and direction to the assumption that k_2^T (s = o) may be assumed to be equal to k_f. When this assumption is not made, then the solution is that given by equations (27). In this solution, there appears the quantity $(1 - \varepsilon + \varepsilon')$, the values in which are 0.034, 0.05, and 1.017 for ε, ε', and $(1 - \varepsilon + \varepsilon')$, respectively, when the thickness of the lithosphere is taken to be 90 km. Figure 6 plots the predictions of polar wander speed based on equations (27) as a function of a parameter $\Delta = \varepsilon/0.034$. Results are shown not only for $\varepsilon = 0.034$ ($\Delta = 1$) which is appropriate for a lithospheric thickness of 90 km, in which case $k_2^T(s = 0) = 0.9263$, but also for significantly smaller values of ε including the value $\varepsilon = 0$ ($\Delta = 0$) so as to investigate the "smoothness" of the transition in the results from the value $\varepsilon = 0$ which obtains when k_2^T (s = 0) is

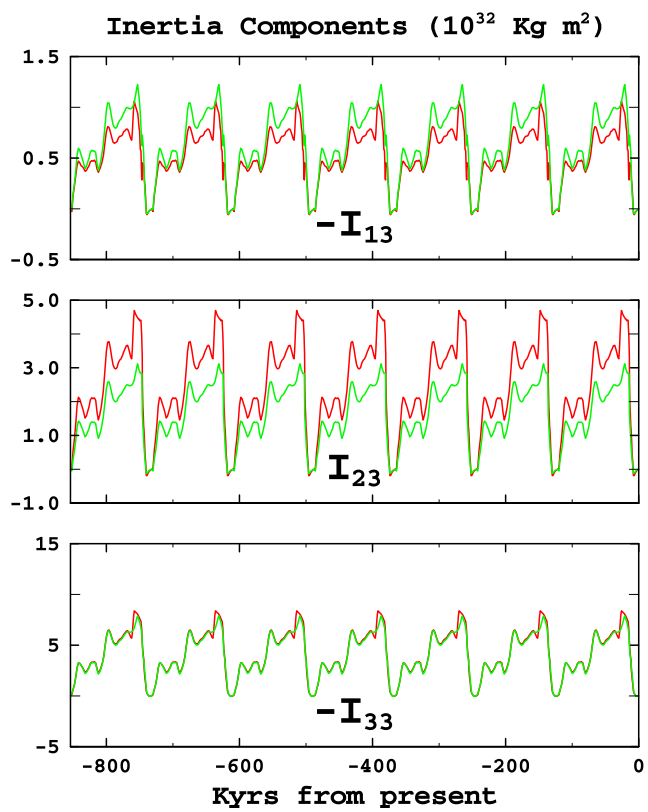

Figure 5. ICE-5G (red) and ICE-4G (green) based model histories for the variation of the I_{13}^R, I_{23}^R, and I_{33}^R components of the inertia tensor for a model history that assumes that seven cycles of glaciation and deglaciation have occurred with an approximate period of 100 kyr. For the purpose of the calculations described in this paper the late Pleistocene glacial-interglacial cycle is assumed to have been precisely periodic. Since the system exhibits a fading memory of its past, this should not have a profound influence on our conclusions. The superscript "R" denotes the fact that the time series for the elements of the inertia tensor shown are the variations that would be characteristic of the ice age cycle if the Earth were entirely rigid has been suppressed on the individual plots.

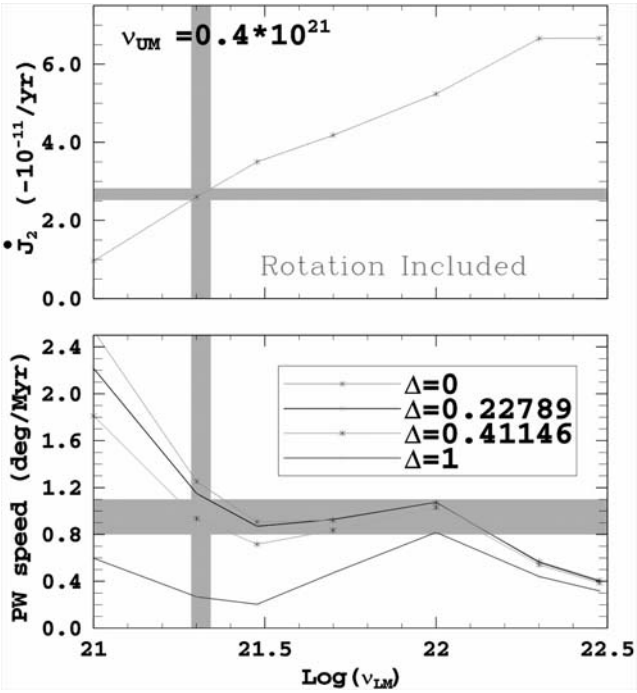

Figure 6. Predictions of $\dot{J}_2$ and polar wander speed for two-layer models of the radial variation of mantle viscosity in which the upper mantle value is held fixed at 0.4×10^{22} Pa s and the lower mantle value beneath a depth of 660 km is varied through the range 10^{21} to$10^{22.5}$ Pa s. The predictions of polar wander speed are shown for several values of the parameter Δ that measures the magnitude of the difference between the fluid Love number of the Earth k_f and the zero frequency asymptotic value of the tidal k Love number of degree 2. Inspection of the polar wander speed predictions demonstrates that the value $\Delta = 1$ is incompatible with the viscosity contrast between upper and lower mantles required by the $\dot{J}_2$ observation.

assumed to be equal to k_f, through the values $\varepsilon = 0.016$ ($\Delta = 0.41146$) corresponding to $k_f = 0.9414$ and $\varepsilon = 0.0078$ ($\Delta = 0.22789$) corresponding to $k_f = 0.9382$ (the value assumed in MW) that would characterize the Earth model if the lithospheric thickness L were assumed to be equal to zero insofar as the infinite time rotational response of the system is concerned. Inspection of the results on Figure 6 shows that in the limit $\Delta \rightarrow 0$ the result agrees very closely with the previous results shown on Figure 1 in the sense that both polar wander speed and the nontidal acceleration are very nearly fit by the same two-layer model of the radial viscoelastic structure although the result for $\Delta = 0.41146$ gives the best fit. Furthermore the preferred value of the lower mantle viscosity is the same value of approximately 2×10^{21} Pa s as previously inferred. Also evident by inspection of Figure 6, however, is the fact that the solution is modified only very slightly when either of the finite nonzero values of Δ are assumed that correspond to a vanishing value of the lithospheric thickness in the infinite time limit insofar as the rotational response of the planet to the tidal forcing is concerned. In fact, the finite nonzero value of $\Delta = 0.41146$ appears to provide the best fit. This further establishes that the Equivalent Earth Model based solution of *Peltier* [1982] and *Wu and Peltier* [1984] provides a very good approximation to the exact solution and that no instability of the mathematical structure (as suggested in MW) is involved. However, it is also evident that if the influence of finite nonzero lithospheric thickness on the infinite time response to the rotational forcing is included ($\Delta = 1$), then it is not possible to simultaneously fit both observables using the same model of the radial viscoelastic structure. Models that include this influence in the two-layer models significantly underpredict the polar wander speed for a radial viscoelastic structure that fits the nontidal acceleration.

[22] Because it is only the polar wander speed datum that is sensitive to the value of Δ, it is of interest to determine whether or not the assumed value of the upper mantle viscosity has any significant influence on this result and whether the redistribution of the ocean load associated with the changing rotation results in any similar sensitivity. Figure 7 provides the results of analyses performed to investigate these sensitivities in terms of the same two-layer models. Results are shown for models based on the assumption of an upper mantle viscosity of either 0.4 or 1×10^{21} Pa s and for models that either include or exclude the impact of the redistribution of water over the global ocean due to the changing rotation. Inspection of these results will show that these sensitivities are modest. It will be clear, however, that the influence of the redistribution of water due to the changing rotation is important in enabling the models to fit both observables with the same viscoelastic structure. This influence reduces the present-day speed prediction by just the amount, for either choice of upper mantle viscosity, that is required to establish this consistency for all three models in which it is assumed that it is the effectively zero value of lithospheric thickness that governs the infinite time response to the rotational forcing.

4.2. Differences in Model Predictions With Realistic Radial Viscosity Structures

[23] In the recent paper by *Peltier* [2007b], a large number of sensitivity studies of the impact on polar wander speed and direction were described in which the VM2 model of the radial viscoelastic structure was fixed and the impact of slight changes in the ICE-5G loading history were investigated, including a switch to the ICE-4G precursor model. All of these analyses were based on the application of the Equivalent Earth Model approach. The sensitivities investigated included the influence of the timing of the end of the Neoglacial readvance of the Greenland Ice Sheet and the influence of modern melting of ice from this region such as has been documented to be occurring through recent analysis of the time-dependent gravity field data being delivered by the GRACE satellite system [e.g., *Velicogna and Wahr*, 2005; *Peltier*, 2009]. These analyses further confirm that the ICE-5G(VM2) model with $\Delta = 0$ provides an excellent fit to the observations although the sensitivities are such that the observations may prove extremely useful in further confirming the action of modern rates and locations of land ice melting.

[24] For the purposes of this paper it will suffice to show in Figures 8a and 8b the predictions of polar wander speed and direction for the ICE-5G(VM2) model based on

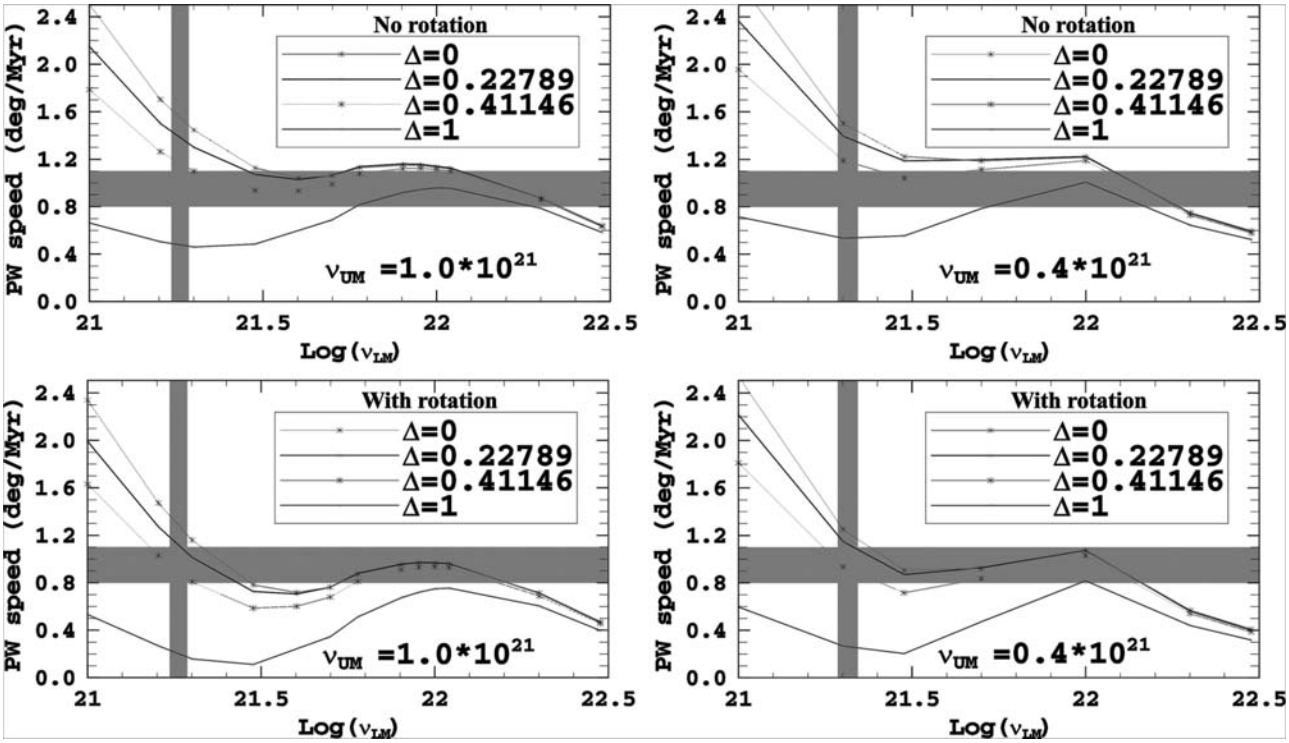

Figure 7. Polar wander speed predictions as in Figure 6 but demonstrating the sensitivity of the results to plausible variations in the upper mantle viscosity and to the incorporation or otherwise of the redistribution of water in the ocean basins that is forced by the impact of the polar wander process itself.

equations (27) as a function of the parameter $\Delta = \varepsilon/0.034$. Figures 8a and 8b differ from one another in that, for the purpose of the former calculations, it has been assumed that the Neoglacial readvance of ice on Greenland that began in the mid-Holocene period has continued up to the present, whereas in Figure 8b it is assumed that this readvance ceased 2000 years ago. Focusing first on Figure 8a, in the limit $\Delta \rightarrow 0$ the result for the present-day (t = 0) polar wander speed, although somewhat fast, is close to the result obtained using the original version of the theory for which k_2^T (s = 0) = k_f is assumed. However, as ε increases toward the value 0.034 (and Δ increases toward 1) that is characteristic of the model in which, even in the limit of infinite time, the lithosphere is assumed to maintain its rigidity, there occurs a continuous transition in the speed of true polar wander, such that the speed of TPW is reduced from that predicted by the "equivalent Earth model" formulation by a factor of ~5 for the value of ε appropriate to the ICE-5G (VM2) model with an elastically intact lithospheric thickness of 90 km ($\Delta = 1$). For the value of Δ appropriate for a lithospheric thickness of zero the result is less significantly reduced. This agrees with the results for the previously discussed two-layer viscosity models and suggests that an excellent way of discriminating between the two different formulations of the theory is through the polar wander speed predictions that follow from the alternative formulations. $\Delta \approx 0$ fits the observation, $\Delta = 1$ does not. The predictions of present-day polar wander direction are also a strong function of Δ as shown by Figure 8a (middle), with the angle for $\Delta = 1$ being hopelessly removed from the observed direction. The results for the present-day predictions of both polar wander speed and direction as a function of Δ are summarized in Figure 8a (right).

[25] The results shown on Figure 8b illustrate the impact on the polar wander speed and direction predictions caused by eliminating the Neoglacial readvance of Greenland ice by 2000 years before present. The most apparent affect concerns the marked impact on the present-day prediction of polar wander direction. Although still unacceptably removed from the modern day observed direction in the case $\Delta = 1$, elimination of the readvance has at least returned it to the correct quadrant.

[26] An appropriate summary of the results of this section would be simply to note that the application of fully realistic models of the radial viscoelastic structure further confirm the results obtained with the two-layer models. However, there does appear to be sufficient latitude in the model to allow the rotational observables to be employed as an additional constraint on the modern distribution and rates of land ice melting as previously investigated by *Peltier* [1998, 2007b]. Further refinement of such analyses should prove interesting and will be reported elsewhere.

5. A Further Test of the Validity of the Theory: Holocene Relative Sea Level Histories

[27] One additional way that we might imagine testing the quality of the theory is one that relies on the global patterns of postglacial relative sea level change that are predicted by the different versions of the calculation. These patterns are best illustrated by global predictions of the present-day rate of relative sea level rise that would be expected to be

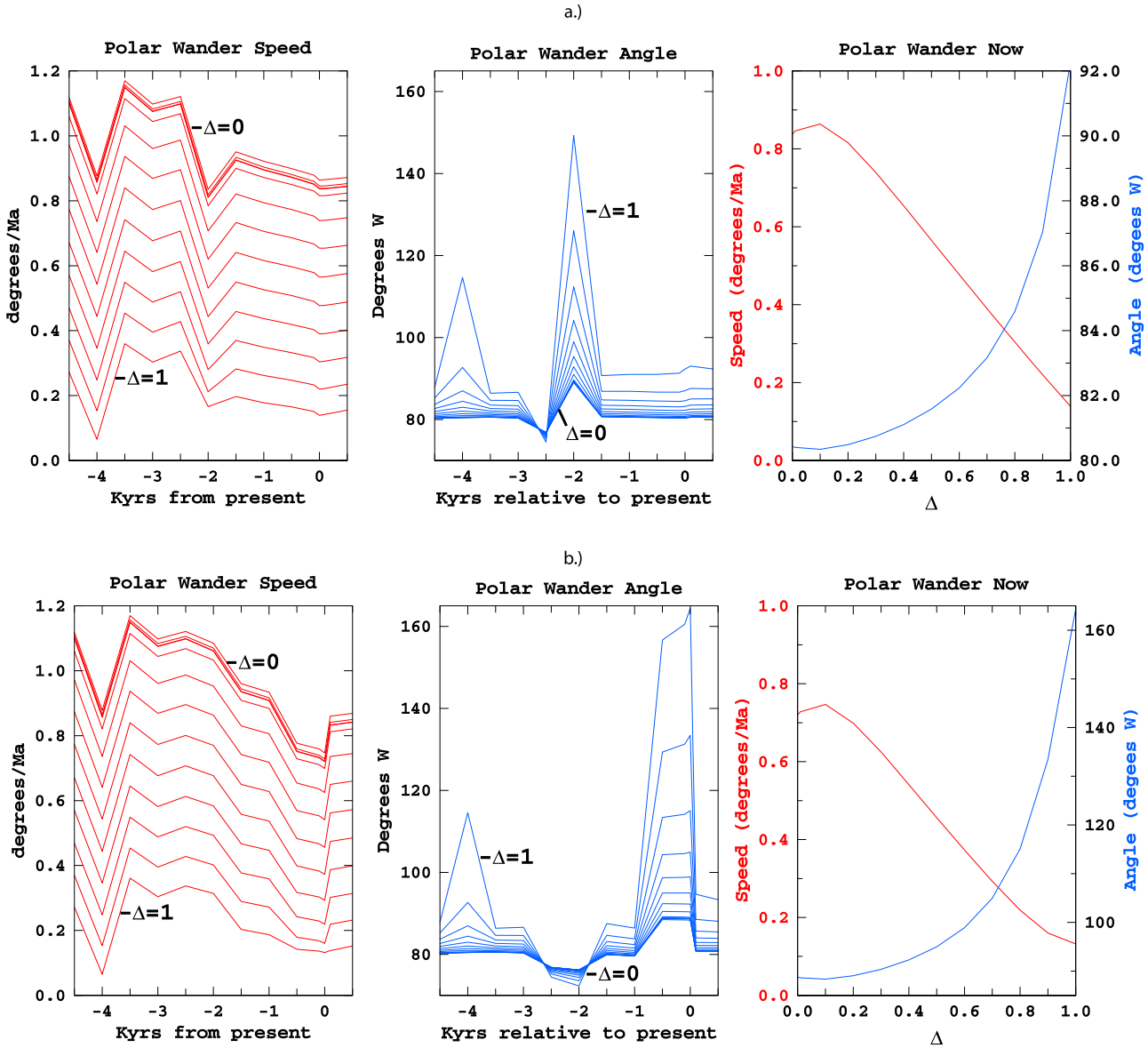

Figure 8. (a) The histories of the evolution with time of polar wander speed and direction from 5 ka before present until 1 kyr into the future, respectively, as a function of the magnitude of the deviation of k_2^T ($s = 0$) from k_f. As explicitly shown on Figure 2, this deviation is a function of lithospheric thickness L. As will be clear on the basis of inspection of Figure 8a (left), as $1 - k_2^T$ (s = 0)/k_f increases in magnitude from zero, the predicted speed of polar wander decreases. The sequence of values of the parameter Δ for which results are shown is (0, 10^{-3}, 10^{-2}, 0.1–1.0 in steps of 0.1). For a finite lithospheric thickness of 90 km this decrease in speed is by a factor of ~2. Figure 8a (right) shows the present-day predicted speed and direction of true polar wander as a function of a parameter Δ which is defined such that $\Delta = 1$ corresponds to the maximum deviation of k_2^T ($s = 0$) from k_f for the assumed value of L. Inspection of Figure 8a (right) will show that although both the speed and direction predictions are marginally acceptable under the equivalent Earth model assumption of *Munk and MacDonald* [1960], for $\Delta = 1$ the predictions are hopelessly discordant with the observations. (b) Same as for Figure 8a but for the version of the ICE-5G model in which the Neoglacial readvance of the Greenland Ice Sheet is assumed to have stopped by 2 ka. It will be noted that this has a profound impact on the large misfit to the observed polar wander angle which is apparent in Figure 8a when this influence is included.

observed as a secular rate of change on a tide gauge installed in a coastal location if the only contribution to relative sea level history were that due to the continuing impact of the GIA process. Figure 9 [from *Peltier*, 2007b] shows Mollwiede projections of the global map of this prediction for ICE-4G and ICE-5G models both including and excluding the impact of rotational feedback with $\Delta = 0$. These predictions have been made by solving equation (1) using the "full glacial cycle" methodology for incorporation of the influence of coastline migration discussed by

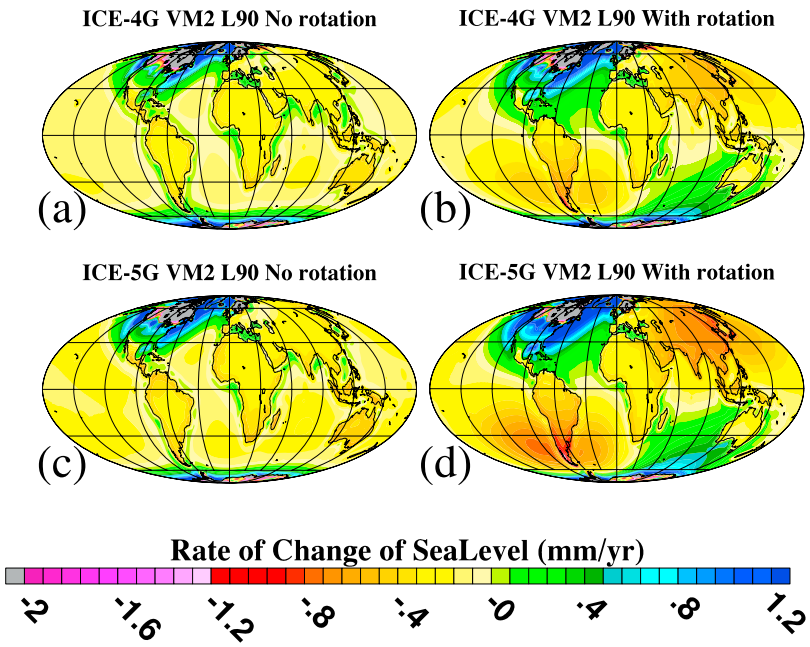

Figure 9. Comparison of the predictions of the (a and b) ICE-4G (VM2) and (c and d) ICE-5G (VM2) models of the present-day rate of relative sea level rise both including and excluding the influence of rotational feedback as described by the second term in the integrand of the triple convolution integral in equation (1). Note that the influence of rotational feedback has the form of a spherical harmonic of degree 2 and order 1 which exists as a consequence of the dominant role played in the feedback process by the polar wander component of the rotational response to the GIA process (see equations (4c) and (4d)). Also evident is the fact that this feedback is stronger in model ICE-5G (VM2) than it is in ICE-4G (VM2).

Peltier [2005]. Inspection of Figure 9 clearly shows that the impact of rotational feedback is such as to superimpose on the pattern predicted by either model, a modification that has the form of a spherical harmonic of degree 2 and order 1 as expected on the basis of the work of *Dahlen* [1976]. This is a consequence of the fact that the dominant impact of rotational feedback is due to the influence of true polar wander, as will be clear on the basis of inspection of equations (4). The ω_3 perturbation to the angular velocity of the planet controls the impact on sea level history of the GIA induced change in the length of day. This influence is negligible. The ω_1 and ω_2 perturbations, on the other hand, control the polar wander contribution and it will be clear on the basis of equation (3) that this will appear as a forcing of spherical harmonic degree 2 and order 1 form. Noticeable also on the basis of Figure 9 is the fact that the magnitude of this impact is more intense in the ICE-5G (VM2) model than it is in the ICE-4G (VM2) model, consistent with the fact that the polar wander speed predicted for this model is higher than for ICE-4G (VM2).This difference can be exploited to examine the extent to which the feedback effect is adequately represented in the original version of the theory of *Peltier* [1982] and *Wu and Peltier* [1984]. Since it is in the regions centered within the 4 "bull's eyes" of the spherical harmonic degree 2 and order 1 pattern that the influence of rotational feedback will be most apparent, it is to these regions that we must look to examine its consequences.

[28] *Peltier* [2007a, 2007b] described a sequence of very detailed analyses that demonstrate the crucial importance that rotational feedback plays in enabling the theory to fit Holocene histories of post glacial sea level change. These analyses, all of which were performed for the limiting case $\Delta = 0$, demonstrated that the data from within each of the extrema of the degree 2 and order 1 pattern were best fit by the ICE-5G model with feedback. In the absence of the action of this feedback, very important qualitative features of the observations were inexplicable. In Figure 10 a subset of these earlier analyses are revisited in which results for $\Delta = 1$ are compared to the results obtained for the case $\Delta = 0$ for the ICE-5G(VM2) model with rotational feedback. Also shown on Figure 10, on which theory and observations are intercompared for sites near two of the southern hemisphere extrema of the degree 2 and order 1 pattern, are predictions of the ICE-4G(VM2) model with rotational feedback and for the ICE-5G(VM2) model without rotational feedback. Inspection of these results demonstrates that the influence of rotational feedback is absolutely required if the theory is to fit the observations and that the best fit to all such records is delivered by the ICE-5G(VM2) model with feedback. Furthermore, because the predictions of this model for the $\Delta = 1$ version of the theory (shown as the sequences of filled red circles) are essentially identical with those for $\Delta = 0$, it will be clear that Holocene relative sea level records cannot be employed to discriminate between which version of the theory is preferred by the observations. This is the first test of this sensitivity using a mathematically exact theory of the impact of finite Δ on Earth's evolving rotational state. In order to test for the influence of this impact we are obliged to seek observations

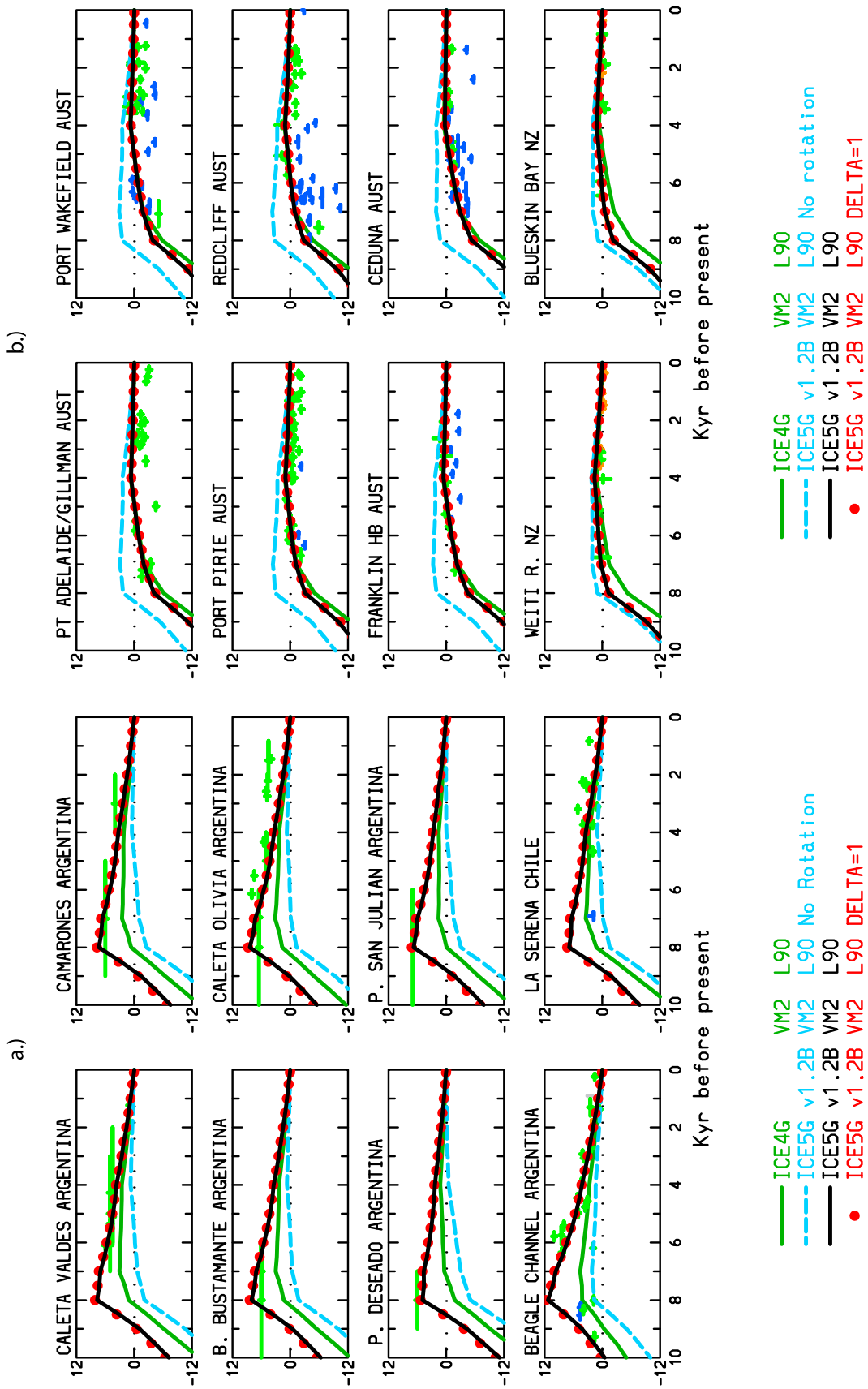
a.)
b.)
CALETA VALDES ARGENTINA
CAMARONES ARGENTINA
PT ADELAIDE/GILLMAN AUST
PORT WAKEFIELD AUST
B. BUSTAMANTE ARGENTINA
CALETA OLIVIA ARGENTINA
PORT PIRIE AUST
REDCLIFF AUST
P. DESEADO ARGENTINA
P. SAN JULIAN ARGENTINA
FRANKLIN HB AUST
CEDUNA AUST
BEAGLE CHANNEL ARGENTINA
LA SERENA CHILE
WEITI R. NZ
BLUESKIN BAY NZ
12
0
-12
10
8
6
4
2
0
Kyr before present
ICE4G VM2 L90
ICE5G v1.2B VM2 L90 No Rotation
ICE5G v1.2B VM2 L90
ICE5G v1.2B VM2 L90 DELTA=1
ICE4G VM2 L90
ICE5G v1.2B VM2 L90 No rotation
ICE5G v1.2B VM2 L90
ICE5G v1.2B VM2 L90 DELTA=1

Figure 10

that are more sensitive than relative sea level history to this influence.

6. GRACE Satellite Observations of GIA: Time-Dependent Stokes Coefficients of Degree 2 and Order 1

[29] The direct observations of the time dependence of the gravitational field of the planet by the GRACE satellite system [*Tapley et al.*, 2004] offers a means, in principle, by which we might directly test the importance of finite Δ on the GIA process. The utility of these data is investigated in detail in what follows through a sequence of steps that address the question from several different perspectives.

6.1. Compatibility of the ICE-5G(VM2) Model With the GRACE Observations

[30] It will be useful to begin this discussion of the GRACE data by first demonstrating the quality of the fit to the GRACE observations over the North American continent that is provided by the ICE-5G (VM2) model. The results of this original analysis of data from the Center for Space Research (CSR) is based on all data up to and including January 2008 which consist of 60 consecutive monthly sets of Stokes coefficients on the basis of which the secular variation of the gravitational field over the continent may be determined. The data processing procedure applied to the data involves the following sequence of analysis steps:

[31] 1. The raw data are downloaded from http://podaac.jpl.nasa.gov/grace/data_access.html.

[32] 2. The data to be employed from the CSR are restricted to maximum spherical harmonic degree and order equal to 60. The Stokes coefficients are converted to surface mass rate coefficients required to express the rate of change of the gravitational field in terms of the time rate of change of the thickness of an equivalent layer of water at the Earth's surface. This involves conversion of the geoid height (Stokes) coefficients to mass rate coefficients through the operation:

$$C_\mathrm{mass}(l,m) = C_\mathrm{geoid}(l,m)\left(\rho_{avg.earth}/\rho_{water}\right) \cdot [(2l+1))/3(1+k_{e_elas}(l))] \tag{29}$$

in which the C_mass(l,m) and the C_geoid(l,m) are either the C(l,m) or the S(l,m) Stokes coefficients.

[33] 3. The correlated error filter of *Swenson and Wahr* [2006] is applied to smooth the coefficients of order m with a quadratic polynomial in degree l with a moving window of width equal to 6. This window clearly cannot be applied for $l < 3$ or for $l > 57$. The filter is applied only for order $m > 8$ as suggested by Swenson and Wahr. After smoothing, the coefficients are converted back from mass rate coefficients to Stokes coefficients.

[34] 4. Each discrete time series of monthly values of the Stokes coefficients is then fit by least squares to a function consisting of a constant bias plus a linear trend plus three periodic components consisting of unique amplitude and phase for each having periods of 365.25 days, 182.625 days and 161 days. This is an 8 term fit in general but our software allows for testing the influence of the number of harmonic terms employed in the fit. Detailed discussions of the influence of the specific parameterization of the time dependence employed on the inferred secular drift of the gravitational field is provided by *Peltier* [2009].

[35] 5. The coefficient of the linear term is taken to define the secular rate of change in each Stokes coefficient.

[36] 6. Normally the coefficients must be corrected before comparison with the results of GIA predictions. This is done by subtracting from the mass rate versions of the Stokes coefficients the values of the equivalent coefficients produced by the Global Land Data Assimilation Scheme (GLDAS) as described by *Rodell et al.* [2004]. These coefficients represent the contributions to the surface mass rate due to land surface hydrological processes. Once decontaminated by this influence the resulting field is normally smoothed by application of a Gaussian filter with a half width of 500 km as described by *Wahr et al.* [1998]. The sensitivity of the results obtained to the assumed width of the filter is also provided by *Peltier* [2009]. Certain Stokes coefficients may also be replaced if they are known not to be accurately determined by the GRACE system itself (e.g., the time dependence of the coefficient of degree 2 and order 0 which is apparently still more accurately determined by Satellite Laser Ranging).

[37] In order to illustrate the quality of the intercomparisons of the GLDAS corrected GRACE observations with the predictions of the ICE-5G (VM2) model, Figure 11a shows the GLDAS corrected GRACE observations over the North American continent and Greenland for surface mass rate. In Figure 11b the same predicted mass rate field is shown based on the prediction of the ICE-5G (VM2) model

Figure 10. (a) Model-data intercomparisons for eight sites from the southern portion of the east coast of the South American continent. These are the same locations from this region discussed at length by *Rostami et al.* [2000] and *Peltier* [2007b] where detailed location data and information on data sources are provided. RSL history predictions based on equation (1) are shown for four model variants ICE-5G (VM2) with rotational feedback and $\Delta = 0$(black), ICE-5G (VM2) without rotational feedback (blue), ICE-4G (VM2) with rotational feedback and $\Delta = 0$(green), and finally ICE-5G(VM2) with rotational feedback and $\Delta = 1$(red dots), respectively. Notable based on the comparisons at these southern coastal sites is that the data strongly prefer the ICE-5G(VM2) model with rotational feedback of the two models that include rotational feedback. However, since the red dotted curve is exactly coincident with the black curve, the data cannot by invoked to say anything concerning the preferred value of Δ. (b) Same as Figure 10a but showing model-data intercomparisons for the Australia–New Zealand region. Inspection of these intercomparisons demonstrates that, as expected based on the results shown on Figure 9, the nature of the influence of rotational feedback is opposite to that observed at the South American locations. At these locations the data are less able to discriminate between the two models that include the influence of rotational feedback, presumably because these sites are insufficiently close to the degree 2 and order 1 "bull's eye" evident on Figure 9.

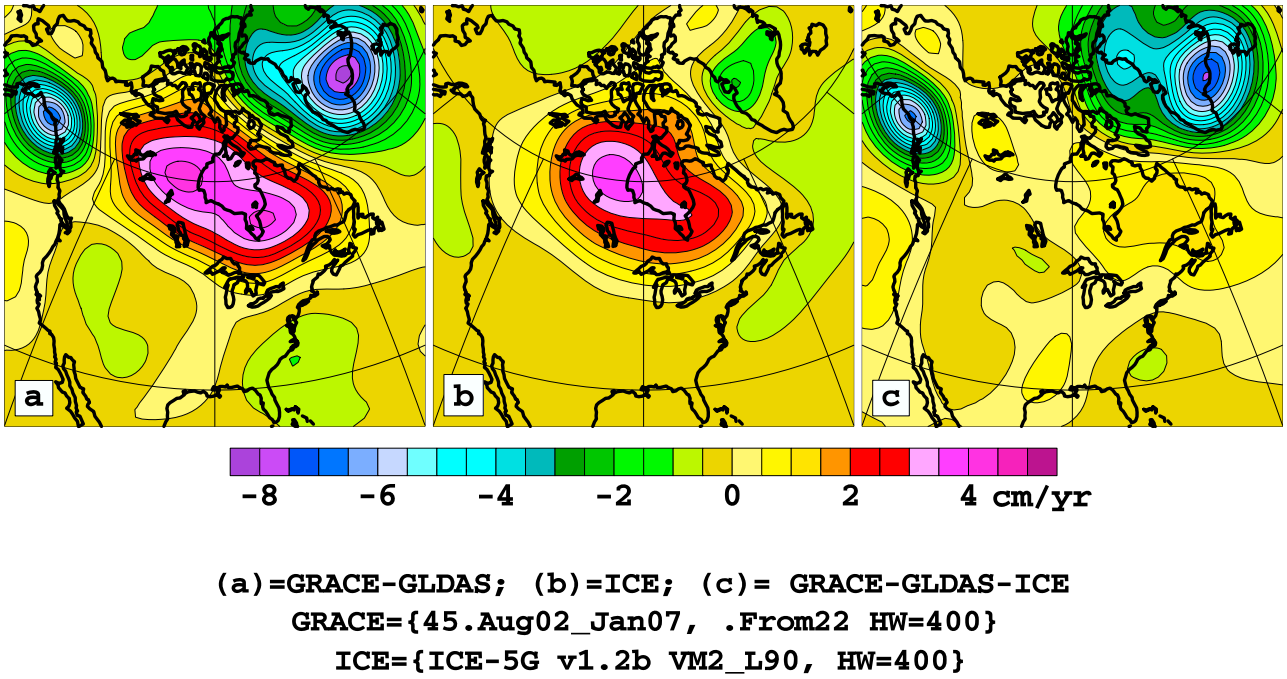

Figure 11. (left) GRACE observation of the time-dependent gravity field over North America corrected for surface hydrology is denoted GRACE-GLDAS in terms of the time rate of change of the thickness of an equivalent layer of water at Earth's surface. (middle) ICE-5G (VM2) GIA prediction of this field. (right) The difference between these two fields, observed minus predicted. The degree 2 and order 1 Stokes coefficients have been eliminated from both. The good first-order fit of the theoretical prediction to the observations subject to this assumption is obvious.

while Figure 11c shows the difference between the observed and theoretically predicted mass rate fields [see also *Peltier*, 2007a; *Peltier and Drummond*, 2008]. In producing each of these fields, the C(2,1) and S(2,1) Stokes coefficients have been eliminated from both theory and observations by employing in the comparison only coefficients of degree 2 and order 2 and higher. It will be clear on the basis of this comparison that the ICE-5G (VM2) model very accurately predicts what the GRACE satellite has seen over the portion of Canada and the United States that was once covered by the Laurentide Ice Sheet. When the theoretical prediction is subtracted from the observed field, the dominant anomaly associated with the deglaciation of the ancient Laurentide Ice Sheet complex is almost entirely eliminated. This is important as the ICE-5G (VM2) model was published by *Peltier* [2004] prior to the time that the GRACE data became available. The residuals that remain over Greenland and the high mountains of Alaska after subtraction of the prediction of the GIA model are associated with the currently ongoing loss of land ice in these regions that is due to high latitude global warming of the lower atmosphere caused by the increasing load of atmospheric greenhouse gases. These inferred rates of mass loss can be mapped directly into a corresponding rate of global sea level rise. Detailed new calculations of the inferred rates of global sea level rise are recorded by *Peltier* [2009]. At this point it is important to note that the ICE-5G (VM2) model of the GIA process is constrained by observations from a period of time during which these high rates of land ice melting near the poles were inactive. If Earth rotation were significantly influenced by this impact of modern greenhouse gas induced global warming, we would not expect the degree 2 and order 1 time-dependent Stokes coefficients being observed by GRACE to be predictable by the ICE-5G (VM2) model. The model would nevertheless remain an accurate model of late Pleistocene ice age influence and therefore the best possible instrument for application to the problem of correcting modern geodetic measurements, such as those being delivered by GRACE, for ancient ice age influence.

6.2. ICE-5G (VM2) GIA Predictions and the Closure of the Global Sea Level Rise Budget

[38] An important additional result that is useful to record here on the basis of the global prediction for the present-day mass rate field that is delivered by the ICE-5G (VM2) model is that for the average over the ocean basins of the rate of change of the thickness of an equivalent layer of water ("mass rate" in Table 1). In Table 1 several predictions are recorded of this average based on variations on the analysis procedure involving the range of latitudes over which the average is computed or, most importantly, by either including or excluding the contribution from the degree 2 and order 1 Stokes coefficients. Also shown in Table 1, for the same set of model assumptions, are the corresponding predictions of the average over the oceans of the rate of inflation (deflation) of the geoid (sea level), a quantity that is observed using the observations being made by the altimetric satellites TOPEX/POSEIDON and Jason-1. Given both entries in Table 1, it is possible to determine

Table 1. Inferences of the Average Over the Ocean Basins of the Present-Day Rate of Increase of Geoid Height (Sea Level, Denoted dGeoid) That Is Predicted by the ICE-5G(VM2) Model of the Glacial Isostatic Adjustment Process[a]

Gaussian Half Widths	Coefficients Excluded	Maximum Degree and Order	Range of Latitude	Average Mass Rate Over the Oceans (mm yr^{-1})	Average dGeoid Over the Oceans (mm yr^{-1})
No filter	none	120	±60°	−1.98	−0.32
400 km	none	120	±60°	−1.90	−0.32
No filter	(2,1)	120	±60°	−1.43	−0.28
400 km	(2,1)	120	±60°	−1.35	−0.28
No filter	none	120	±66°	−1.99	−0.32
400 km	none	120	±66°	−1.88	−0.32
No filter	(2,1)	120	±66°	−1.41	−0.27
400 km	(2,1)	120	±66°	−1.30	−0.27
No filter	none	120	±90°	−1.80	−0.30
400 km	none	120	±90°	−1.65	−0.29
No filter	(2,1)	120	±90°	−1.32	−0.26
400 km	(2,1)	120	±90°	−1.17	−0.26

[a]This is the rate that must be subtracted from the TOPEX/POSEIDON and JASON-1 altimetric observations of the rate of global sea level rise in order to estimate the rate due to greenhouse gas warming of the lower atmosphere (the result for the ICE-5G(VM2) model updates the result first published by *Peltier* [2001]). Also shown are results for the average over the ocean basins of the present-day rate of increase of the equivalent thickness of a layer of water (denoted mass rate) predicted by the ICE-5G(VM2) model. This is the correction that must be subtracted from the GRACE data to correct for the influence of the GIA process so that the altimetric observation may be separated into its steric and water mass components.

whether or not it is possible to close the sea level budget. This budget may be represented schematically as follows:

$$\text{Altimetric rate (TOPEX/POSEIDON} - \text{GIA)} = \text{Mass rate (GRACE} - \text{GIA)} + \text{Steric rate (e.g., Levitus)}$$

Notable is the fact that both the altimetric rate and the mass rate must be corrected for the contribution to them due to the influence of the glacial isostatic adjustment process. The steric contribution to the global rate of sea level rise is directly known on the basis of the oceanographic observations of, e.g., *Levitus et al.* [2005] or, more recently insofar as subdecadal variability is concerned, on the basis of Argo float data [*Roemmich and Owens*, 2000]. In this regard the most important results displayed in Table 1 are those that obtain when the degree 2 and order 1 Stokes coefficients are eliminated from the analysis so that the feedback of the changing state of Earth's rotation is eliminated. It will be observed that the latter effect is extremely important. According to *Cazenave et al.* [2009], if the altimetric correction to the TOPEX/POSEIDON global rate of sea level rise measurement is taken to be approximately −0.30 mm yr^{-1} (see Table 1), as first described by *Peltier* [2001], then the average rate of increase in the thickness of an equivalent layer of water over the ocean basins must be close to −1.90 mm yr^{-1} in order to establish closure of the sea level budget. Their analysis could be construed to deliver an independent estimate of what the GRACE correction for GIA must be in order that the sea level budget, as observed over the GRACE era, be closed. Since the average of the raw GRACE mass rate data over the oceans delivers an effectively zero value for this rate, the GIA correction must itself equal the value required to close the budget. Inspection of the results in Table 1 for the ICE-5G (VM2) model demonstrates that this is, in fact, the value predicted by the ICE-5G(VM2) model but only if the full influence of the degree 2 and order 1 Stokes coefficients predicted for the ICE-5G (VM2) model is included. Furthermore, this positive outcome is based on the assumption that the rotational response of the planet to surface mass load forcing is that based on the recognition that the effective thickness of the elastic lithosphere is zero in the infinite time limit insofar as the rotational response is concerned. An extremely important caveat to this analysis, however, is that the very large contribution to the global rate of sea level rise due to the melting of small ice sheet and glaciers by *Meier et al.* [2007] is accurate. Their inference of the rate that has been active over the period during which the GRACE satellites have been flying is 1.1 mm yr^{-1}, almost double their earlier estimates [e.g., *Dyurgerov and Meier*, 1997]. A further detailed analysis of the closure of the sea level budget over the GRACE era is given by *Peltier* [2008]. Given that the ICE-5G (VM2) model is constrained by observations from an earlier epoch during which greenhouse-gas-induced polar and high-elevation land ice melting was not occurring at a significant rate it is expected that the model, including its predictions of the rotation influenced time-dependent Stokes coefficients, would provide an accurate representation of ice age influence. There is nevertheless an important issue as to how accurately these coefficients are being measured by GRACE, an issue to which we next turn.

6.3. Accuracy of the GRACE Observations of the Degree 2 and Order 1 Stokes Coefficients

[39] It is of considerable interest, in the further exploration of the utility of the GRACE data, to understand the extent to which the quality of the comparison of theory and observation in section 6.1 would be compromised by the incorporation of the degree 2 and order 1 Stokes coefficients that have been suggested by the main modeling centers to be fixed by the GRACE observations themselves. To this end, Figure 12a shows the map of the field of geoid height time dependence that is predicted by the degree 2 and order 1 Stokes coefficients alone as these are determined by

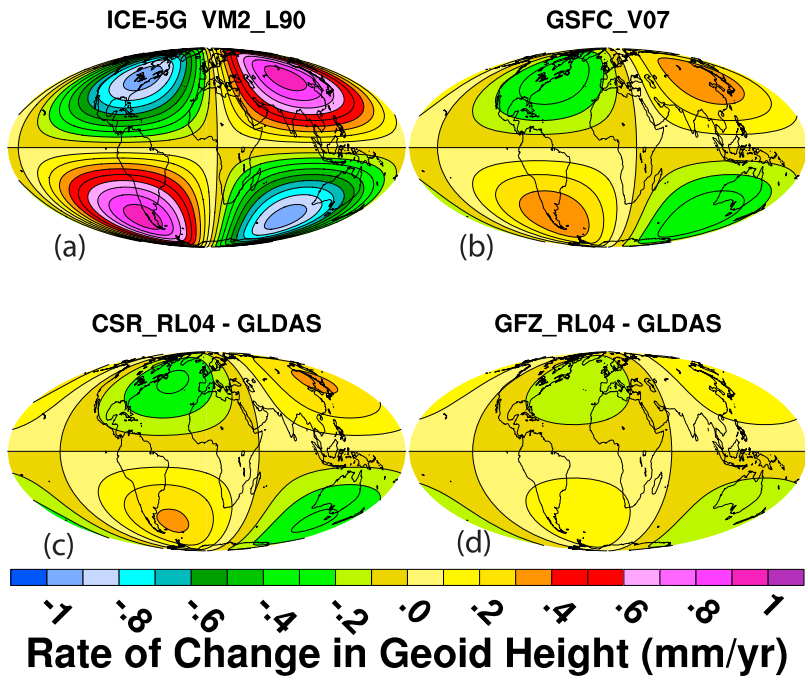

Figure 12. (a) ICE-5G (VM2) prediction of the degree 2 and order 1 map of the present-day rate of change of geoid height is denoted simply as ICE-5G. (b) The original new inference labeled GSFC_V07 that is discussed in the text together with (c and d) the predictions of CSR and GFZ.

the same ICE-5G(VM2) model of the GIA process that so well fits the observations in the absence of contributions from these coefficients. Notable is the fact that this places one of the 4 extrema of the pattern over the southern tip of the South American continent where it is required in order to allow the theory to fit the extremely highstands of the sea that are characteristic of this coastal region during mid-Holocene time (as discussed in section 5).

[40] In order to usefully compare this component of the prediction of the ICE-5G (VM2) model with the GLDAS corrected GRACE observations, it is necessary to understand that the very long wavelengths corresponding to the degree 2 and order 1 time dependence could be a challenge for the satellite system to accurately observe. In order to improve the rate of convergence of the recovery of these Stokes coefficients from the observations, the Center for Space Research (CSR) has employed a methodology in which a time-dependent background gravity model is introduced from which the satellite data are employed to infer a deviation. For the degree 2 and order 1 Stokes coefficients, this background model consists of an assumption that a first estimate of them may be obtained by simply rotating the degree 2 and order 0 Stokes coefficient in the direction and at the observed speed of polar wander as obtained on the basis of appropriate Earth orientation time series [see, e.g., *Gross and Vondrák*, 1999]. The expressions for the time rates of change of the C(2,1) and S(2,1) Stokes coefficients that this assumption delivers are as follows:

$$\dot{C}_b(2,1) = \sqrt{3}\,\dot{x}\,\overline{C(2,0)} = -0.337 \times 10^{-11}\mathrm{yr}^{-1} \tag{30a}$$

$$\dot{S}_b(2,1) = -\sqrt{3}\,\dot{y}\,\overline{C(2,0)} = 1.606 \times 10^{-11}\mathrm{yr}^{-1} \tag{30b}$$

By including these values in the forward model, the CSR analysis delivers final values for these coefficients as the sum of these forward modeled values and the deviation from them (see the appropriate entry in Table 2) which are as follows:

$$\dot{C}_{\mathrm{CSR}}(2,1) = -1.80 \times 10^{-11}\mathrm{yr}^{-1} \tag{31a}$$

$$\dot{S}_{\mathrm{CSR}}(2,1) = 1.18 \times 10^{-11}\mathrm{yr}^{-1} \tag{31b}$$

Now the corresponding GLDAS coefficients that must be employed to correct the sum of the coefficients in equations (30a), (30b), (31a) and (31b) are as follows:

$$\dot{C}_{\mathrm{GLDAS}}(2,1) = 0.093 \times 10^{-11}\ \mathrm{yr}^{-1} \tag{32a}$$

$$\dot{S}_{\mathrm{GLDAS}}(2,1) = -0.56 \times 10^{-11}\ \mathrm{yr}^{-1} \tag{32b}$$

It is notable that these required corrections to the satellite inferred values are not small in the case of S(2,1), which raises the question as to whether or not the hydrology model should be incorporated in the forward modeling of the observations as are the ocean, atmosphere and tides themselves. Combining these estimates as (31a), (31b), (32a) and (32b) delivers the CSR derived GRACE estimates of the degree 2 and order 1 Stokes coefficients that are to be compared to the predictions of the model of the GIA process that so accurately fits the observations when these coefficients are entirely neglected and which produces an accurate prediction of the GIA correction required in order to ensure closure of the budget of global sea level rise. The

Table 2. Inferences of the Time Dependence of the Degree 2 and Order 1 Stokes Coefficients Based on the Raw Range Rate Data[a]

Coefficient and Analysis Center Version	Forward Model Summary	Rate From Time Series of GRACE Monthly Estimates (yr^{-1})	Specific Forward Modeled Rate (yr^{-1})	Total Rate GRACE Estimate and Specific Forward Modeled (yr^{-1})
C20 GSFC_V05	atmosphere, ocean, tides	1.23E-11	0.0	1.23E-11
C20 GSFC_V06	atmosphere, ocean, tides, hydrology	1.49E-11	0.0	1.49E-11
C20 GSFC_V07	atmosphere, ocean, tides hydrology, ICE5G	0.96E-11	1.52E-11 (ICE-5G)	2.48E-11
C20 CSR_RL04	atmosphere, ocean, tides	−3.30E-11	1.16E-11 (IERS)	−2.14E-11
C20 GFZ_RL04	atmosphere, ocean, tides	2.67E-11	1.16E-11 (IERS)	3.84E-11
C21 GSFC_V05	atmosphere, ocean, tides	−1.65E-11	0.0	−1.65E-11
C21 GSFC_V06	atmosphere, ocean, tides, hydrology	−1.47E-11	0.0	−1.47E-11
C21 GSFC_V07	atmosphere, ocean, tides hydrology,ICE5G	−0.38E-11	−1.30E-11 (ICE-5G)	−1.68E-11
C21 CSR_RL04	atmosphere, ocean, tides	−1.464E-11	−3.37E-12 (IERS)	−1.80E-11
C21 GFZ_RL04	atmosphere, ocean, tides	−8.95E-12	−3.37E-12 (IERS)	−1.23E-11
S21 GSFC_V05	atmosphere, ocean, tides	1.20E-11	0.0	1.20E-11
S21 GSFC_V06	atmosphere, ocean, tides, hydrology	1.76E-11	0.0	1.76E-11
S21 GSFC_V07	atmosphere, ocean, tides, hydrology, ICE5G	−5.00E-11	7.67E-11 (ICE-5G)	2.67E-11
S21 CSR_RL04	atmosphere, ocean, tides	−4.27E-12	1.61E-11 (IERS)	1.18E-11
S21 GFZ_RL04	atmosphere, ocean, tides	−1.32E-11	1.61E-11 (IERS)	2.84E-12

[a]The raw data are archived by the Goddard Space Flight Center (GSFC), the Center for Space Research (CSR), and the Geoforshung Zentrum (GFZ) based, in the case of CSR and GFZ, on the RL04 release of the GRACE time-dependent gravity data. The GSFC analyses are all original analyses of the raw data, V05 employing the same forward modeling procedure as the other two centers and V06 employing a modified procedure in which the GLDAS land surface hydrology model is also included in the forward modeling procedure. The V07 analysis also includes the ICE-5G (VM2) model of the GIA process as well as the GLDAS hydrology in the forward model. The new GSFC results pertain to the period April 2003 through May 2007.

map of these estimates is shown in Figure 12 (bottom left) which is based on the following values:

$$\dot{C}_{\mathrm{GIA_GRACE}}(2,1) = -1.89 \times 10^{-11}\ \mathrm{yr}^{-1} \tag{33a}$$

$$\dot{S}_{\mathrm{GIA_GRACE}}(2,1) = 1.74 \times 10^{-11}\ \mathrm{yr}^{-1} \tag{33b}$$

The values of the these Stokes coefficients "observed" according to the CSR analysis of the GRACE satellite data are to be compared to those predicted by the ICE-5G (VM2) model of the GIA process which are as follows, a map for which is also shown in Figure 12 (top left).

$$\dot{C}_{\mathrm{ICE\text{-}5G(VM2)}}(2,1) = -1.30 \times 10^{-11}\ \mathrm{yr}^{-1} \tag{34a}$$

$$\dot{S}_{\mathrm{ICE\text{-}5G(VM2)}}(2,1) = 7.67 \times 10^{-11}\ \mathrm{yr}^{-1} \tag{34b}$$

From Figure 12 it is evident that there are very large differences between the ICE-5G (VM2) model predictions and the GRACE observations according to the CSR interpretation. Inspection of the results listed in Table 2 shows that the interpretation is actually similar to the results obtained from the analyses performed by the GFZ. These differences are primarily although not entirely due to the very large misfit between the GIA predicted value of $\dot{S}_{ICE\text{-}5G(VM\ 2)}$ (2,1) and the $\dot{S}_{GIA_GRACE}$ (2,1) observation.

[41] It might be thought that a possible explanation of the large discrepancy between theoretical predicted Stokes coefficients and the inferences by these data centers in terms of the revised version of the theory of the rotational response to the GIA process presented in section 3. In this modified form of the theory the parameter DELTA is employed to measure the importance of the inhibiting influence of finite lithospheric thickness on the rotational response to the GIA process. One way to test whether the incorporation of this influence might resolve the large discrepancy between the observed and predicted values of the Stokes coefficient S21-dot (equivalent to dS21/dt, the derivative of S21 with respect to time t) is simply to compute the changes to C21-dot and S21-dot that are induced by finite values of DELTA. When we fix the ice-loading history to ICE-5G and the radial profile of mantle viscosity to VM2 (a viscosity structure, the upper 1200 km or so of which was recently confirmed by the analyses of *Paulson et al.* [2007], then we find the following values of these coefficients for the 4 values of DELTA for which results were previously discussed:

$$\mathrm{DELTA} = 0.0,\ \mathrm{C21\text{-}dot} = -1.25 \times 10^{-11},\ \mathrm{S21\text{-}dot} = 7.69 \times 10^{-11}$$
$$\mathrm{DELTA} = 0.22789,\ \mathrm{C21\text{-}dot} = -1.19 \times 10^{-11},\ \mathrm{S21\text{-}dot} = 7.41 \times 10^{-11}$$
$$\mathrm{DELTA} = 0.41146,\ \mathrm{C21\text{-}dot} = -0.96 \times 10^{-11},\ \mathrm{S21\text{-}dot} = 6.25 \times 10^{-11}$$
$$\mathrm{DELTA} = 1.0,\ \mathrm{C21\text{-}dot} = -0.18 \times 10^{-11},\ \mathrm{S21\text{-}dot} = 2.40 \times 10^{-11}$$

This demonstrates, as will be clear on the basis of the previously discussed theory, that as DELTA increases the predicted values of both Stokes coefficients decrease commensurately. It follows that, if one believes the CSR inferred values of these coefficients to be accurate, then the theory cannot be corrected so as to fit them by increasing DELTA since by using this degree of freedom to minimize the error in S21-dot, one introduces a similarly unacceptable error in C21-dot.

[42] A second possible way out of the difficulty posed by the misfit of theory to both the CSR and GFZ versions of the analysis of the GRACE observations (see Table 2) may be simply to assume that GRACE may be unable to provide an accurate measurement of the degree 2 and order 1 Stokes coefficients. We have explicitly tested this possibility in the following way, with the results of this test also listed in Table 2. A completely new series of reductions of the raw GRACE range rate data has been performed using three different flavors of the analysis procedure. The difference between these two methodologies lies in the assumptions made for the purpose of forward modeling. In the first case, labeled GSFC-V05 in Table 2, only the conventional fields are included in the forward analysis procedure, namely, those describing the atmospheric, oceanographic and tidal contributions to the time dependence of the Stokes coefficients. In the second, for which results are labeled GSFC-V06 in Table 2, the forward model also includes the GLDAS hydrology model of the contribution to the time dependence of the degree 2 and order 1 Stokes coefficients. A third reduction of the data has also been performed in which the ICE-5G (VM2) predictions of the Stokes coefficients are also included in the forward model. These results are labeled GFSC-V07 in Table 2. Also shown in Table 2 are the final inferred values of the time dependence of the Stokes coefficients of degree 2 and order 1 as well as that of degree 2 and order 0. As will be clear on the basis of inspection of the results in Table 2, there is no evidence of extremely large differences between the result for S21-dot between GSFC-06 and GSFC-07 as would be expected if GRACE were not capable of providing any significant constraint on these Stokes coefficients. We must therefore conclude that the large difference in the prediction of the S21-dot coefficient by the ICE-5G (VM2) model is physically significant. However, it is also noticeable that there are very large differences between the values of S21-dot inferred by the different modeling centers. Most noticeable is the order of magnitude difference between the inferred value of this coefficient by GFZ (0.284×10^{-11} yr^{-1}) and that by GSFC V07 (2.80×10^{-11} yr^{-1}). In contrast the inferred values of C21-dot by the different modeling centers are much more stable, the largest difference in this case being between the GSFC V06 result (-1.14×10^{-11} yr^{-1}) and the CSR result (-1.80×10^{-11} yr^{-1}). Given these differences we are obliged to continue to entertain the possibility that GRACE may be singularly ill suited as a measurement system for the inference of the Stokes coefficient S21-dot. In this regard it is especially interesting that the mean value of the 5 available estimates of the C21-dot coefficient, namely, -1.43×10^{-11} yr^{-1}, is so close to the value predicted of the ICE-5G (VM2) model, namely, -1.30×10^{-11} yr^{-1}, implying an error of less than 10% in this coefficient. The closest of the five estimates of the S21-dot coefficient to that predicted by ICE-5G (VM2) is that delivered by the GSFC V07 model in which the result for ICE-5G(VM2) was included in the forward modeling procedure. It is also important to note the very significant dispersion among the 5 estimates of the C20-dot coefficient. These vary wildly, even in regards to sign, with the CSR estimate being -2.14×10^{-11} yr^{-1} and the GFZ estimate being $+3.84 \times 10^{-11}$ yr^{-1}. Although the new GSFC estimates are more tightly clustered than this, they too vary from 0.88×10^{-11} yr^{-1} to 1.23×10^{-11} yr^{-1} (Table 2). The ICE-5G(VM2) prediction of this coefficient is 1.52×10^{-11} yr^{-1} so that, again, the GSFC V07 estimate that included the ICE-5G (VM2) prediction in the forward analysis is closest to this prediction of the GIA model. In section 7 we have attempted to summarize the conclusions that follow from the full suite of analyses presented in this paper.

7. Conclusions

[43] The detailed theory required to accurately predict the rotational response to the glacial isostatic adjustment process, when the difference between the observed fluid Love number of the planet and the zero frequency limit of the prediction of the viscoelastic field theory of *Peltier* [1974] is included, has been fully developed in this paper (see also the "grey" literature discussion by *Peltier* [2008]; this reference is referred to as appearing in gray literature since the volume containing it simply records the contents of the papers presented at the 15th International Conference on Laser Ranging). Subject to the assumption that in this limit the surface lithosphere should exert no influence on the rotational response, since it is broken by the process of surface plate tectonics, the full theory delivers predictions for the secular variations in both the length of day and polar motion that are consistent with the requirements of "paleo" space geodetic observations. This is in spite of the fact that the zero frequency limit of the field theory does not exactly fit the observed value of the fluid Love number. Nevertheless, the misfit to this parameter is so small that the effect is minimal. However, if the entire surface lithosphere is treated as an intact elastic shell in the full theory and in the zero frequency limit, then the prediction of polar wander speed and direction cannot explain the "paleo" observations for the same model of the radial viscoelastic structure as is required to fit the secular variation in the length of day. It is therefore established that the suggestion in MW that the misfit of the zero frequency limit of the viscoelastic field theory of *Peltier* [1982] and *Wu and Peltier* [1984] to the observed flattening of the planet's shape, invalidates the results of previous analyses, is incorrect. Their statement to the effect that this original form of the theory was based on an unstable mathematical formulation has also been shown to be false.

[44] It has furthermore been shown that observations of Holocene relative sea level history have insufficient sensitivity to the difference between the fluid Love number and the zero frequency limit of the prediction of the field theory to enable one to discriminate between models that do or do not include this influence. This is in spite of the fact that the influence of rotational feedback on RSL observations near the centers of the rotation induced spherical harmonic degree 2 and order 1 pattern is highly significant [*Peltier*, 2002b, 2005, 2007a]. This characteristic of the pattern of rotational influence is enforced by the dominance of true polar wander over that due to the changing length of day.

[45] New analyses of the time dependence of the gravitational field of the planet, as this is being measured by the GRACE satellite system, demonstrates that this system is

able to provide useful constraints on the time rates of change of the Stokes coefficients of degree 2 and order 1 which are controlled by the strength of the influence of rotational feedback on the response of the planet to the late Pleistocene glaciation-deglaciation cycle. However, there is also a suggestion that the GRACE system is somewhat less sensitive to the coefficient S21-dot than it appears to be to the coefficient C21-dot. This suggestion deserves further investigation.

[46] We suggest that the key to understanding why the otherwise excellent ICE-5G (VM2) model of the glacial isostatic adjustment process does not deliver an accurate fit to the GRACE observations of the time-dependent degree 2 and order 1 Stokes coefficients is simply that, during the GRACE era of the past 5 years, the rotational state of the planet has been significantly altered by the ongoing loss of land ice from the polar and high-elevation regions of the planet. As shown explicitly in section 5, the action of such modern ice sheet melting has a significant impact on Earth rotation. Models of modern land ice melting such as those constrained by GRACE itself [e.g., *Cazenave et al.*, 2009; *Peltier*, 2009] for the polar regions and by *Meier et al.* [2007] for the small ice sheets and glaciers, must be shown to pass the test provided by the GRACE observations. However, the ICE-5G (VM2) model, and the modest improvements to it that are currently under construction, are precisely the models required to filter ice age influence from these modern space geodetic observations. This has now been clearly demonstrated by the fact that this model provides the required correction to the GRACE observed mass rate over the oceans that is needed to ensure closure of the sea level budget [*Cazenave et al.*, 2009; *Peltier*, 2009]. The following paragraph from MW (last paragraph of their section 2) is therefore shown to be entirely erroneous:

> Peltier (2004) has recently presented predictions of the GIA contribution to present-day geoid rates using a preferred Earth model (VM2) characterized by a lower mantle viscosity varying in the range 2-3 $\times$ 10^{21} Pa s. These predictions, motivated by the impending availability of high-precision GRACE satellite constraints, were based on the traditional TPW theory. We conclude that the large (2,1) TPW feedback signal evident in them (Peltier, 2004; fig. 22) is over estimated by at least a factor of 2.

They clearly believe that a model of the GIA process that has been constrained to fit "paleo" geodetic observations, including late Holocene observations of sea level history, should also fit the observations currently being made by the GRACE satellite. If it were not for the fact that the influence of modern land ice melting strongly influences the GRACE observations, this would be reasonable. This significant misunderstanding has already had serious consequences. In the recent paper of *Leuliette and Miller* [2009], for example, they discuss the application of GRACE measurements to the sea level budget closure problem. They accept as a reasonable estimate for the GIA-related mass rate correction over the oceans, a value of -1.0 mm yr^{-1} which is approximately a factor of 2 smaller in magnitude than the value delivered by the ICE-5G (VM2) model listed here in Table 1 and discussed more fully by *Peltier* [2009]. The *Peltier* [2009] value has previously been accepted by *Cazenave et al.* [2009] as being required to achieve closure of the budget. Although *Leuliette and Miller* [2009] claim that they also achieve closure of the budget using a value for the GIA correction of -1.0 mm yr^{-1}, a value attributed to *Paulson et al.* [2007], it will be clear that their own analysis would be markedly improved if they were to employ the ICE-5G(VM2) value for the GIA correction. The value of the mass rate correction over the oceans delivered by the Paulson et al. model has been produced using the erroneous theory advocated in MW. Our conclusion, contrary to the statement in the above quoted paragraph from MW, is that "the large (2,1) TPW feedback signal evident in them (*Peltier*, 2004; fig. 22)" is, in fact, now recognized as being required on the basis of sea level budget closure analysis.

[47] Interesting work clearly remains to be done using the theory for GIA-related rotational influence that has been further elaborated herein. Analyses to be reported elsewhere will address the issue as to whether the models of modern land ice melting due to the influence of the greenhouse effect are fully compatible with the GRACE observations. These modern sources of land ice melting will have to be superimposed on the loads associated with the most recent glacial cycle in order that a complete forward model can be constructed for comparison with GRACE and other observations. This will require the development of detailed models of the contribution of small ice sheets and glaciers to augment those from the great polar ice sheets that have recently been reanalyzed by *Peltier* [2009].

[48] **Acknowledgments.** The work reported in this paper is a contribution to the Polar Climate Stability Network which is supported by the Canadian Foundation for Climate and Atmospheric Science. Further support has been provided by NSERC Discovery grant 9627. Support for the GRACE analysis was provided by NASA under the GRACE Science Team program.

References

Argus, D. F., and R. S. Gross (2004), An estimate of motion between the spin axis and the hotspots over the past century, *Geophys. Res. Lett.*, *31*, L06614, doi:10.1029/2004GL019657.

Broecker, W. S., and J. van Donk (1970), Insolation changes, ice volumes, and the δ^{18}O record in deep sea cores, *Rev. Geophys. Space Phys.*, *8*, 169–198, doi:10.1029/RG008i001p00169.

Cazenave, A., K. Dominh, S. Guienhut, E. Berthier, W. Llovel, G. Ramillien, M. Ablain, and G. Larnicol (2009), Sea level budget over 2003–2008: A re-evaluation from GRACE space gravimetry, satellite altimetry and Argo, *Global Planet. Change*, *65*(1–2), 83–88, doi:10.1016/j.gloplacha.2008.10.004.

Cheng, M., and B. D. Tapley (2004), Variations in the Earth's oblateness during the past 28 years, *J. Geophys. Res.*, *109*, B09402, doi:10.1029/2004JB003028.

Cheng, M., R. J. Eanes, C. K. Shum, B. E. Schutz, and B. D. Tapley (1989), Temporal variations in low degree zonal harmonics from Starlette orbit analysis, *Geophys. Res. Lett.*, *16*, 393–396, doi:10.1029/GL016i005p00393.

Clark, J. A., W. E. Farrell, and W. R. Peltier (1978), Global changes in postglacial sea levels: A numerical calculation, *Quat. Res.*, *9*, 265–287, doi:10.1016/0033-5894(78)90033-9.

Cox, C., and B. F. Chao (2002), Detection of large scale mass redistribution in the terrestrial system since 1998, *Science*, *297*, 831–833, doi:10.1126/science.1072188.

Dahlen, F. A. (1976), The passive influence of the oceans upon the rotation of the Earth, *Geophys. J. R. Astron. Soc.*, *46*, 363–406.

Domack, E., et al. (2005), Stability of the Larsen B ice shelf on the Antarctic Peninsula during the Holocene epoch, *Nature*, *436*, 681–685, doi:10.1038/nature03908.

Dyurgerov, M. B., and M. F. Meier (1997), Mass balance of mountain and sub-polar glaciers: A new assessment for 1961–1990, *Arct. Alp. Res.*, *29*, 379–391, doi:10.2307/1551986.

Dziewonski, A. M., and D. L. Anderson (1981), Preliminary reference Earth model, *Phys. Earth Planet. Inter.*, *25*, 297–356, doi:10.1016/0031-9201(81)90046-7.

Farrell, W. E. (1972), Deformation of the Earth by surface loads, *Rev. Geophys.*, *10*, 761–797, doi:10.1029/RG010i003p00761.

Farrell, W. E., and J. A. Clark (1976), On postglacial sea level, *Geophys. J. R. Astron. Soc.*, *46*, 647–667.

Gross, R. S., and J. Vondrák (1999), Astrometric and space-geodetic observations of polar wander, *Geophys. Res. Lett.*, *26*, 2085–2088, doi:10.1029/1999GL900422.

Lambeck, K., and J. Chappell (2001), Sea level change through the last glacial cycle, *Science*, *292*(5517), 679–686, doi:10.1126/science.1059549.

Leuliette, E. W., and L. Miller (2009), Closing the sea level rise budget with altimetry, Argo, and GRACE, *Geophys. Res. Lett.*, *36*, L04608, doi:10.1029/2008GL036010.

Leventer, A., E. Domack, R. Dunbar, J. Pike, C. Stckley, E. Maddison, S. Brachfield, P. Manely, and C. McClennan (2006), Marine sediment record from East Antarctica margin reveal dynamics of ice-sheet recession, *GSA Today*, *16*(12), 4–10, doi:10.1130/GSAT01612A.1.

Levitus, S., J. I. Antonov, and T. P. Boyer (2005), Warming of the world ocean, 1955–2003, *Geophys. Res. Lett.*, *32*, L02604, doi:10.1029/2004GL021592.

Meier, M. F., M. B. Dyurgerov, U. K. Rick, S. O'Niel, W. T. Pfeffer, R. S. Anderson, S. P. Anderson, and A. S. Glazovsky (2007), Glaciers dominate sea level rise in the 21st century, *Science*, *317*, 1064–1067, doi:10.1126/science.1143906.

Mitrovica, J. X., J. Wahr, I. Matsuyama, and A. Paulson (2005), The rotational stability of an ice-age Earth, *Geophys. J. Int.*, *161*, 491–506, doi:10.1111/j.1365-246X.2005.02609.x.

Munk, W. H., and G. F. MacDonald (1960), *The Rotation of the Earth*, Cambridge Univ. Press, New York.

Nakiboglu, S. M., and K. Lambeck (1980), Deglaciation effects on the rotation of the Earth, *Geophys. J. R. Astron. Soc.*, *62*, 49–58.

Nakiboglu, S. M., and K. Lambeck (1981), Deglaciation related features of the Earth's gravity field, *Tectonophysics*, *72*, 289–303, doi:10.1016/0040-1951(81)90242-0.

Paulson, A., S. Zhong, and J. Wahr (2007), Inference of mantle viscosity from GRACE and relative sea level data, *Geophys. J. Int.*, *171*, 497–508, doi:10.1111/j.1365-246X.2007.03556.x.

Peltier, W. R. (1974), The impulse response of a Maxwell Earth, *Rev. Geophys. Space Phys.*, *12*, 649–669, doi:10.1029/RG012i004p00649.

Peltier, W. R. (1976), Glacial isostatic adjustment, II: The inverse problem, *Geophys. J. R. Astron. Soc.*, *46*, 669–706.

Peltier, W. R. (1982), Dynamics of the ice-age Earth, *Adv. Geophys.*, *24*, 1–146.

Peltier, W. R. (1985), The LAGEOS constraint on deep mantle viscosity: Results from a new normal mode method for the inversion of viscoelastic relaxation spectra, *J. Geophys. Res.*, *90*, 9411–9421, doi:10.1029/JB090iB11p09411.

Peltier, W. R. (2001), Global glacial isostatic adjustment and modern instrumental records of relative sea level history, in *Sea Level Rise: History and Consequences*, edited by B. C. Douglas, M. S. Kearney, and S. P. Leatherman, pp. 65–96, Academic, New York.

Peltier, W. R. (1994), Ice-age paleotopography, *Science*, *265*, 195–201, doi:10.1126/science.265.5169.195.

Peltier, W. R. (1996), Mantle viscosity and ice-age ice-sheet topography, *Science*, *273*, 1359–1364, doi:10.1126/science.273.5280.1359.

Peltier, W. R. (1998), Postglacial variations in the level of the sea: Implications for climate dynamics and solid-Earth geophysics, *Rev. Geophys.*, *36*, 603–689, doi:10.1029/98RG02638.

Peltier, W. R. (2002a), On eustatic sea level history, Last Glacial Maximum to Holocene, *Quat. Sci. Rev.*, *21*, 377–396, doi:10.1016/S0277-3791(01)00084-1.

Peltier, W. R. (2002b), Global glacial isostatic adjustment: Paleo-geodetic and space-geodetic tests of the ICE-4G (VM2) model, *J. Quat. Sci.*, *17*, 491–510, doi:10.1002/jqs.713.

Peltier, W. R. (2004), Global glacial isostasy and the surface of the ice-age Earth: The iCE-5G (VM2) model and GRACE, *Annu. Rev. Earth Planet. Sci.*, *32*, 111–149, doi:10.1146/annurev.earth.32.082503.144359.

Peltier, W. R. (2005), On the hemispheric origins of meltwater pulse 1a, *Quat. Sci. Rev.*, *24*, 1655–1671, doi:10.1016/j.quascirev.2004.06.023.

Peltier, W. R. (2007a), Postglacial coastal evolution: Ice-Ocean-Solid Earth interactions in a period of rapid climate change, in *Coastline Changes: Interrelations of Climatic and Geological Processes*, edited by J. A. Haarf, W. W. Hay, and D. M. Tetzlaff, pp. 5–28, Geol. Soc. of Am., Boulder, Colo.

Peltier, W. R. (2007b), History of Earth rotation, in *Treatise on Geophysics*, vol. 9, *Evolution of the Earth*, edited by D. Stevenson, pp. 243–293, Elsevier, Oxford, U. K.

Peltier, W. R. (2008), Global glacial isostasy: Target fields for space geodesy, in *Proceedings of the 15th International Workshop on Laser Ranging. Canberra Australia, 16–20 October 2006*, edited by J. Luck et al. pp. 55–68, EOS Space Syst. Pty. Ltd., Canberra.

Peltier, W. R. (2009), Closure of the budget of global sea level rise over the GRACE era: The importance and magnitudes of the required corrections for global glacial isostatic adjustment, *Quat. Sci. Rev.*, *28*, 1658–1674, doi:10.1016/j.quascirev.2009.04.004.

Peltier, W. R., and J. T. Andrews (1976), Glacial isostatic adjustment I; The forward problem, *Geophys. J. R. Astron. Soc.*, *46*, 605–646.

Peltier, W. R., and R. Drummond (2008), The rheological stratification of the lithosphere: A direct inference based upon the geodetically observed pattern of the glacial isostatic adjustment of the North American continent, *Geophys. Res. Lett.*, *35*, L16314, doi:10.1029/2008GL034586.

Peltier, W. R., and R. G. Fairbanks (2006), Global glacial ice-volume and Last Glacial Maximum duration from an extended Barbados Sea Level record, *Quat. Sci. Rev.*, *25*, 3322–3337, doi:10.1016/j.quascirev.2006.04.010.

Peltier, W. R., and X. Jiang (1996), Glacial isostatic adjustment and Earth rotation: Refined constraints on the viscosity of the deepest mantle, *J. Geophys. Res.*, *101*, 3269–3290, doi:10.1029/95JB01963. (Correction, *J. Geophys. Res. 102*, 10,101–10,103, doi:10.1029/97JB00620, 1997).

Peltier, W. R., W. E. Farrell, and J. A. Clark (1978), Glacial isostasy and relative sea-level: A global finite element model, *Tectonophysics*, *50*, 81–110, doi:10.1016/0040-1951(78)90129-4.

Pinot, S., G. Ramstein, S. P. Harrison, I. G. Prentice, J. Guiot, M. Stute, and S. Joussaume (1999), Tropical paleoclimates at the Last Glacial Maximum: Comparison of Paleoclimate Modeling Intercomparison (PMIP) simulations and paleodata, *Clim. Dyn.*, *15*, 857–874, doi:10.1007/s003820050318.

Rodell, M., et al. (2004), The Global Land Data Assimilation System, *Bull. Am. Meteorol. Soc.*, *85*, 381–394, doi:10.1175/BAMS-85-3-381.

Roemmich, D., and W. B. Owens (2000), The ARGO project: Global ocean observations for understanding and predicting climate variability, *Oceanography*, *13*(4), 45–50.

Rostami, K., W. R. Peltier, and M. Mangini (2000), Quaternary marine terraces, sea level changes and uplift history of Patagonia, Argentina: Comparisons with predictions of the ICE-4G (VM2) model of the global process of glacial isostatic adjustment, *Quat. Sci. Rev.*, *19*, 1495–1525, doi:10.1016/S0277-3791(00)00075-5.

Sabadini, R., and W. R. Peltier (1981), Pleistocene deglaciation and the Earth's rotation: Implications for mantle viscosity, *Geophys. J. R. Astron. Soc.*, *66*, 553–578.

Shackleton, N. J. (1967), Oxygen isotope analysis and Pleistocene temperatures re-addressed, *Nature*, *215*, 15–17, doi:10.1038/215015a0.

Shackleton, N. J., and N. D. Opdyke (1973), Oxygen isotope and paleomagnetic stratigraphy of equatorial Pacific core V28-238: Oxygen isotope temperatures and ice volumes on a 10^5-year time scale, *Quat. Res.*, *3*, 39–55, doi:10.1016/0033-5894(73)90052-5.

Stephenson, E. R., and L. V. Morrison (1995), Long term fluctuations in the Earth's rotation: 700 B.C. to A.D. 1990, *Philos. Trans. R. Soc. London, Ser. A*, *351*, 165–202, doi:10.1098/rsta.1995.0028.

Swenson, S., and J. Wahr (2006), Post-processing removal of correlated errors in GRACE data, *Geophys. Res. Lett.*, *33*, L08402, doi:10.1029/2005GL025285.

Tapley, B. D., J. C. Bettadpur, J. C. Ries, P. F. Thompson, and M. Watkins (2004), GRACE measurements of mass variability in the Earth system, *Science*, *305*, 503–505, doi:10.1126/science.1099192.

Velicogna, I., and J. Wahr (2005), Greenland mass balance from GRACE, *Geophys. Res. Lett.*, *32*, L18505, doi:10.1029/2005GL023955.

Vincente, R. O., and S. Yumi (1969), Co-ordinates of the pole (1899–1968) returned to the conventional international origin, *Publ. Int. Lat. Obs. Mizusawa*, *7*, 41–50.

Vincente, R. O., and S. Yumi (1970), Revised values (1941–1961) of the coordinates of the pole referred to the CIO, *Publ. Int. Lat. Obs. Mizusawa*, *7*, 109–112.

Waelbroeck, C., L. Labyrie, E. Michel, J.-C. Duplessy, J. F. McManus, K. Lambeck, E. Balbon, and M. Labracherie (2002), Sea-level and deep water temperature changes derived from benthic foraminifera isotopic records, *Quat. Sci. Rev.*, *21*(1–3), 295–305, doi:10.1016/S0277-3791(01)00101-9.

Wahr, J., M. Molenaar, and F. Bryan (1998), Time variability of the Earth's gravity field: Hydrological effects and their possible detection using GRACE, *J. Geophys. Res.*, *103*, 30,205–30,230, doi:10.1029/98JB02844.

Widder, D. V. (1946), *The Laplace Transform*, 406 pp., Oxford Univ. Press, Cambridge, U. K.

Wu, P., and W. R. Peltier (1984), Pleistocene deglaciation and the Earth's rotation: A new analysis, *Geophys. J. R. Astron. Soc.*, *76*, 202–242.

Yoder, C. F. (1995), Astrometric and geodetic properties of Earth and the solar system, in *Global Earth Physics: A Handbook of Physical Con-*

stants, *AGU Ref. Shelf*, vol. 1, edited by T. J. Ahrens, pp. 1–31, AGU, Washington, D. C.

Yoder, C. F., J. G. Williams, J. O. Dickey, B. E. Schutz, R. J. Eanes, and B. D. Tapley (1983), Secular variation of the Earth's gravitational harmonic J_2 coefficient from LAGEOS and non-tidal acceleration of Earth rotation, *Nature*, *303*, 757–762, doi:10.1038/303757a0.

S. B. Luthcke, NASA Goddard Space Flight Center, Planetary Geophysics Laboratory, Code 698, Greenbelt, MD 20771, USA.

W. R. Peltier, Department of Physics, University of Toronto, Toronto, ON M5S 1A7, Canada. (peltier@atmosp.physics.utoronto.ca)